Ocean Modelling 142 (2019) 101439

Contents lists available at ScienceDirect

Ocean Modelling

journal homepage: www.elsevier.com/locate/ocemod

Composite physical–biological El Niño and La Niña conditions in the California Current System in CESM1-POP2-BEC

Nathalí Cordero-Quirós [a,*], Arthur J. Miller [a], Aneesh C. Subramanian [b], Jessica Y. Luo [c,1], Antonietta Capotondi [d,e]

[a] Scripps Institution of Oceanography, University of California, San Diego, USA
[b] University of Colorado, Boulder, CO, USA
[c] Climate and Global Dynamics, National Center for Atmospheric Research (NCAR), Boulder CO, USA
[d] Cooperative Institute for Research in Environmental Sciences, University of Colorado, Boulder, CO, USA
[e] Physical Sciences Division, NOAA Earth System Research Laboratory, Boulder, CO, USA

ARTICLE INFO

Keywords:
ENSO
California Current System
Composite
Physical–biological interactions

ABSTRACT

El Niño-Southern Oscillation (ENSO) is recognized as one of the potentially predictable drivers of California Current System (CCS) variability. In this study, we analyze a 67-year coarse-resolution (~1°) simulation using the ocean model CESM-POP2-BEC forced by NCEP/NCAR reanalysis winds to develop a model composite of the physical–biological response of the CCS during ENSO events. The model results are also compared with available observations. The composite anomalies for sea surface temperature (SST), pycnocline depth, 0m-100m vertically averaged chlorophyll, 0m-100m vertically averaged zooplankton, 25m-100m vertically averaged nitrate, and oxygen at 200m depth exhibit large-scale coherent relationships between physics and the ecosystem, including reduced nutrient and plankton concentrations during El Niño, and increased nutrient and plankton concentrations during La Niña. However, the anomalous model response in temperature, chlorophyll, and zooplankton is generally much weaker than observed and includes a 1–2 month delay compared to observations. We also highlight the asymmetry in the model CCS response, where composite model La Niña events are stronger and more significant than model El Niño events, which is a feature previously identified in observations of CCS SST as well as in tropical Pacific Niño-4 SST where atmospheric teleconnections associated with ENSO are forced. These physical–biological composites provide a view of some of the limitations to the potentially predictable impacts of ENSO teleconnections on the CCS within the modeling framework of CESM-POP2-BEC.

1. Introduction

The California Current System (CCS) is among the most biologically productive oceanic regions of the world (*e.g.,* Hickey, 1998; Checkley and Barth, 2009; Miller et al., 2015). The configuration of the wind patterns along this Eastern Boundary Upwelling System (EBUS) favors the existence of a large upwelling region that extends from northern Baja California, Mexico, to Oregon and Washington on the U.S. West Coast (*e.g.,* Bakun et al., 2015). This phenomenon establishes the environment as a highly productive region that is subject to local variability, some of which is imprinted by atmospheric and oceanic teleconnections from remote changes in the equatorial Pacific. One of the main physical drivers of CCS interannual variability is the El Niño-Southern Oscillation (ENSO), producing changes in sea surface temperature (SST), upwelling, lateral advection of water masses, pycnocline depth, surface heat flux, freshwater flux, eddy kinetic energy, and other fields. All these variables are known to be forcing agents for ecological conditions and biogeochemical content that affect the state of the ecosystem on ENSO time scales (*e.g.,* Schwing et al., 2005).

There are two main mechanisms by which ENSO drives change in the CCS. The first (local atmospheric variability due to atmospheric teleconnections) is related to the intensification of the Aleutian Low (and associated weakening of the North Pacific High) that enhances poleward flow of warm air along the northeastern Pacific (Niebauer, 1988; Jacox et al., 2015) and suppresses upwelling favorable winds along California coast. The second mechanism (oceanic variability due to remotely driven waves) is related to the equatorial Kelvin-like waves in the tropical ocean excited by the westerly winds and coupled ocean-atmosphere feedbacks during El Niño (McPhaden et al., 1998). These waves propagate eastward across the Equatorial Pacific, and then poleward after colliding with the coast of South America (Chávez and

* Correspondence to: Scripps Institution of Oceanography, University of California, San Diego, La Jolla, CA 92093, USA.
E-mail address: nacorder@ucsd.edu (N. Cordero-Quirós).
[1] Current address: NOAA Geophysical Fluid Dynamics Laboratory, 201 Forrestal Rd, Princeton NJ 08540, USA.

https://doi.org/10.1016/j.ocemod.2019.101439
Received 31 July 2018; Received in revised form 12 August 2019; Accepted 18 August 2019
Available online 30 August 2019
1463-5003/

Coauthors, 2002). They are also potentially generated along the Central American and Baja California coasts by subtropical wind fields altered by the tropical ocean conditions. The remotely-driven wave mechanism also deepens the thermocline and suppresses upwelling of nutrient-rich waters both in the equatorial region and along the North American West Coast (*e.g.,* Frischknecht et al., 2015). The combination of local atmospheric and remote oceanic variability imprinted by ENSO in the CCS plays an important role in understanding the CCS response during these events.

ENSO is known to have predictable components, some of which may significantly impact the CCS and therefore be exploitable for practical predictions (*e.g.,* Jacox et al., 2017). While the effects of El Niño over land in the U.S. are well documented (Gershunov and Barnett, 1998; McPhaden et al., 1998; Wang et al., 2012), its effects over the ocean are less understood, particularly because of limited observations. The CCS is unique because it is one of the most extensively sampled ocean regions (*e.g.,* Bograd and Lynn, 2002; Crawford et al., 2017), with the California Cooperative Oceanic Fisheries Investigations (CalCOFI) providing hydrographic *in-situ* data since the late 1950s, along with various satellite measurements covering the area since the late 1970s. There are many studies that address the ecological effects of particular El Niño events over the CCS (*e.g.,* Bograd and Lynn, 2001; Chávez and Coauthors, 2002; Jacox et al., 2016; Ohman, 2018) using the limited observations that indicate reduction of nutrient and plankton concentrations during warm conditions and vice versa for cold events. However, because of the sparseness of the data in both space and time, there is limited understanding of how consistently these warm and cold ENSO events impact both the physical and biological state of this region (*e.g.,* Di Lorenzo and Miller, 2017, summarize the results of a recent workshop on this topic).

Coupled physical and biogeochemical models represent an important tool for addressing oceanic variability and provide an alternative and complementary approach to using only direct observations for the study of marine ecosystems (*e.g.,* Curchitser et al., 2013; Frischknecht et al., 2015, 2017; Turi et al., 2018). Analyzing the effects of ENSO on the CCS over the entire observational record in conjunction with model simulations may help to quantify how consistently the ENSO events impact the physical and biological system. This can also shed light on how well model forecasts of ENSO variability might be trusted for developing useful outlooks for ecosystem resource management.

In this study, we analyze a 67-year-long physical–biogeochemical simulation driven by observed surface forcing using the oceanic component of the Community Earth System Model (CESM) to study the changes associated with El Niño and La Niña over the CCS. We first characterize the model's anomalous CCS ENSO response as a whole and then develop monthly-mean El Niño and La Niña composites (*cf.,* Turi et al., 2018) for various physical and biogeochemical variables. After comparing the results with available observations, we identify the limitations that can be expected in both the physical and biological regional response to ENSO events, given observed atmospheric forcing and a coarse-resolution ocean model. Although the resolution of this model is coarse, it simultaneously includes the effects of physics, low trophic level ecology, and biogeochemistry, which together provide a large-scale synergistic perspective on the response compared to what can be assessed with simpler biological models or with observations alone. This model-analysis approach allows us to better illustrate the limited predictability of the physical–biological behavior of the CCS during ENSO events (*e.g.,* Ohman et al., 2013; Franks et al., 2013).

2. Data and methods

2.1. Model

We employ a 67-year (1949–015) hindcast simulation with 1° resolution and global coverage from the Community Earth System Model version 1 (CESM1; Hurrell et al., 2012). The ocean component is the Parallel Ocean Program, version 2 (POP2; Danabasoglu et al., 2012), and the sea ice component is the Community Ice Code, version 4 (CICE4; Jahn et al., 2011). The ocean biogeochemistry is based on the Biogeochemical Elemental Cycling (BEC; Moore et al., 2002, 2004, 2013) model embedded in POP2. The ocean and ice components are forced by atmospheric reanalysis data, following the Coordinate Ocean-Ice Reference Experiments II (CORE2; Large and Yeager, 2009) protocol that uses winds from the NCEP-NCAR reanalysis, except for the tropical band (30°S-30°N) that uses 20th Century Reanalysis (20CRv2) (Griffies et al., 2009); Yeager et al., 2018. Monthly means of all variables were available to be used in our subsequent analysis.

The ecosystem component consists of three explicit phytoplankton functional types, representing diatoms, diazotrophs, and small phytoplankton, with coccolithophores included as an implicit fraction of the latter, plus one zooplankton group. It also includes dynamic Carbon:Chlorophyll ratios and photoadaptation (Geider et al., 1997, 1998) as well as light and multiple nutrient (N, P, Si, Fe) co-limitation. BEC simulates the elemental cycles of nitrogen, phosphate, silicate, and iron, leading to skillful representations of oceanic chlorophyll, nutrients, and oxygen over the global ocean (Moore et al., 2002, 2004, 2013).

2.2. Observational data

Model validation for sea surface temperature anomalies (SSTa) was made using observations from the Hadley Centre Ice-Sea Surface Temperature (HadISST, Rayner et al., 2003) from January 1949 to December 2015. The model SSTa are also compared over a single point at La Jolla, CA, using observations from the Shore Stations Program (http://scripps.ucsd.edu/programs/shorestations/shore-stations-data/) during three different El Niño Events. The skewness of ENSO over the CCS is analyzed qualitatively using probability density functions (PDF) of SSTa derived from the modeled fields over the whole period (1949–2015) and SSTa from the HadISST for the same years.

Observed chlorophyll data was obtained from the Sea-viewing Wide Field-of-view-Sensor (SeaWiFS) Level 3 standard mapped image (SMI), with a monthly temporal resolution and 9.2 km resolution (O'Reilly et al., 2000). We used chlorophyll from 1998 to 2010 to compare with the model response for that same period. The model chlorophyll fields were averaged down to a depth of 25 m as a proxy to compare with satellite surface chlorophyll concentration that measures over the local oceanic optical depth.

2.3. Methods

The hindcast simulation covers the time period January, 1949, to December, 2015. To focus on ENSO-related time scales, we eliminated the strong signals in the CCS associated with decadal (and longer, including trends) variability from the model fields and the observations. We used a Lanczos high-pass filter with a cutoff frequency of 10 years (following Turi et al., 2018), which successfully removed the low-frequency energy in each variable for both model and observations.

All composite variables were constructed by averaging together each of the selected El Niño and La Niña events identified in the period of the simulation over the 3 months before and the 8 months after (i.e., a 12-month composite) the wintertime (DJF) peak of the event. The years identified as El Niño and La Niña follow the NOAA protocol (NCEP/NOAA, http://origin.cpc.ncep.noaa.gov/products/analysis_monitoring/ensostuff/ONI_v5.php), but only include the moderate-to-strong events and exclude the weak events. In brief, we identify El Niño years as those when Niño-3.4 3-month averaged SSTa $\geq$1.0 °C and La Niña years as those when SSTa ≤ -1.0 °C, where the anomalies persist during both the fall (SON) and winter (DJF) seasons. The resulting El Niño years included in the 12-month composite are: *1951–1952, 1957–1958, 1963–1964, 1965–1966, 1968–1969, 1972–1973, 1982–1983, 1986–1987, 1987–1988, 1991–1992, 1994–1995, 1997–1998, 2002–2003,* and *2009-2010*. The resulting years for the La Niña composite are:

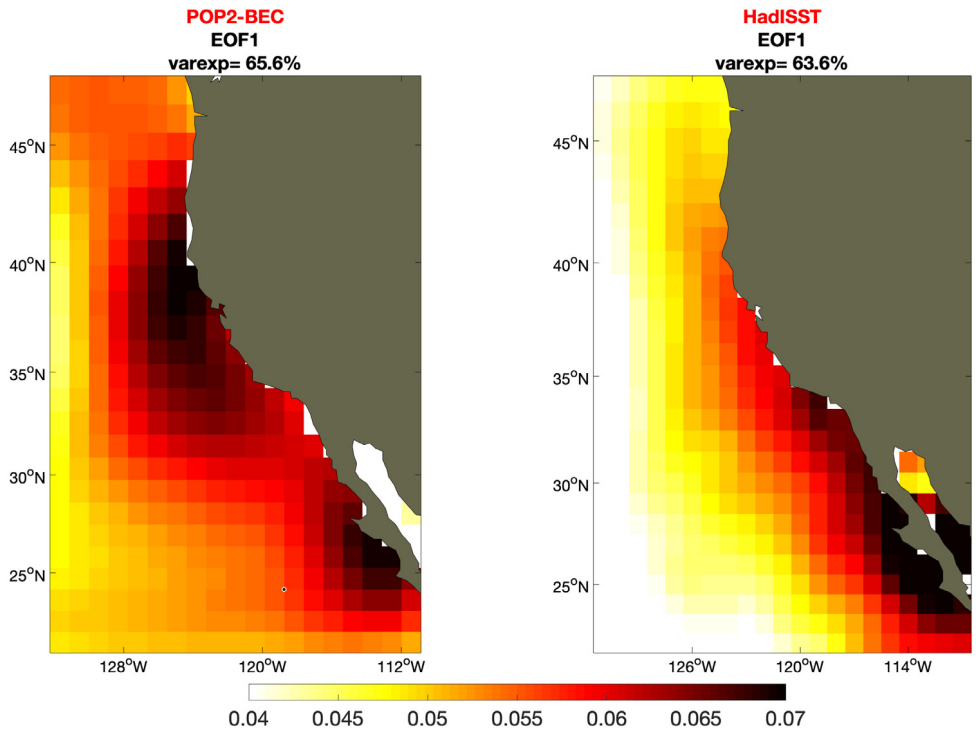

Fig. 1. EOF1 calculated from the full record (1949–2015) of SSTa over the CCS. Left panel shows the EOF from model POP2-BEC. Right panel shows the observed EOF from HadISST.

1949–1950, 1955–1956, 1970–1971, 1971–1972, 1973–1974, 1975–1976, 1983–1984, 1984–1985, 1988–1989, 1995–1996, 1998–1999, 1999–2000, 2007–2008, 2010–2011, and *2011-2012.* This yields a total of 14 El Niño events and 15 La Niña events.

Additional validation of SST fields was made via Empirical Orthogonal Function (EOF) analysis of the SSTa over the CCS. EOF1 from the model (including all months together) and its associated principal component (PC1) were compared to the first observed mode from HadISST and correlated with monthly values of NOAA's Climate Prediction Center (CPC) Oceanic Niño Index (ONI). For the composite results presented below, a total chlorophyll estimate (mg m^{-3}) was calculated as the sum of all three phytoplankton groups, averaged over the top 100 m of the water column to include any potential subsurface chlorophyll maximum. The same method was applied for zooplankton carbon biomass in mmol m^{-3}. Nutrient composites are represented by nitrate concentrations (mmol m^{-3}) averaged between 25 m and 100 m depth, corresponding to the strong vertical gradient in the nitracline. We also compute composite dissolved oxygen concentration (mmol m^{-3}) at a single depth of 200 m. The analysis was made over the CCS region extending from 21°N to 48°N, and from the coast to 132°W.

Anomalies were calculated by subtracting the 12-month climatology from the entire record after high-pass filtering. The 14 El Niño and 15 La Niña years as indicated by the SSTa were used to build the composite anomalies for SST, pycnocline depth (using the $\sigma = 26$ isopycnal surface as a proxy), vertically averaged zooplankton biomass, vertically averaged chlorophyll concentrations, vertically averaged [NO_3], and [O_2] at 200 m depth, which represent key indicators of both physical drivers and ecosystem state. The composites were tested for significance via bootstrap analysis as follows: a hundred composites were randomly computed for each variable and then compared to the composites of El Niño and La Niña obtained from the model. Only those anomalies greater than 2 standard deviations (2σ) of the random distribution are considered to be statistically significant at above the 95% level.

3. Results

3.1. Model validation with SST

As a broad-scale depiction of the overall interannual response of the CCS to the prescribed forcing, Fig. 1 shows the first mode (EOF1) of the SSTa over CCS calculated from the whole record of the model (left panel) and HadISST (right panel), with a 65.6% and a 63.6% of variance explained, respectively. EOF1 in the model dominates the coastal region from southern Baja California to Oregon, showing the coherency between these two regions, but extends further offshore than in observations. EOF1 from HadISST dominates over central and south Baja California, and it is coherent along Baja California and the California coast. Both in model and observations, the first mode of SSTa resembles the well-known pattern developed during warming related to El Niño along the CCS. The principal components (PC1) associated with the first modes are shown in Fig. 2 (top and middle). The PC1 of the model SSTa is well correlated (0.94) with PC1 from HadISST and they are both moderately correlated with the CPC-ONI (Fig. 2, bottom) with coefficients of 0.5 (HadISST) and 0.43 (model), indicating their relevance as the local imprint of ENSO teleconnections from the tropics.

Another broad perspective on the performance of the model in representing interannual CCS variability is the monthly SSTa (°C) averaged over the CCS region for both the model and observations (Fig. 3, top). The correlation between these time series is 0.93, and the RMSE is 0.24, indicating a good agreement in both the timing and magnitude of the variability when averaged over the whole region. However, the model produces a somewhat weaker local response than observed when compared over a single point, which will become more apparent in subsequent analyses. For example, Fig. 3 (bottom) also shows the monthly SSTa from the model and from the Shore Stations Program at La Jolla/Scripps Pier station. Three of the strongest registered El Niño events are shown (1972–1973, 1982–1983 and 1997–1998), each one showing the year before and the year after the wintertime peak (DJF) of El Niño to compare the development and demise of these major events. The model only captures part of the variability of the

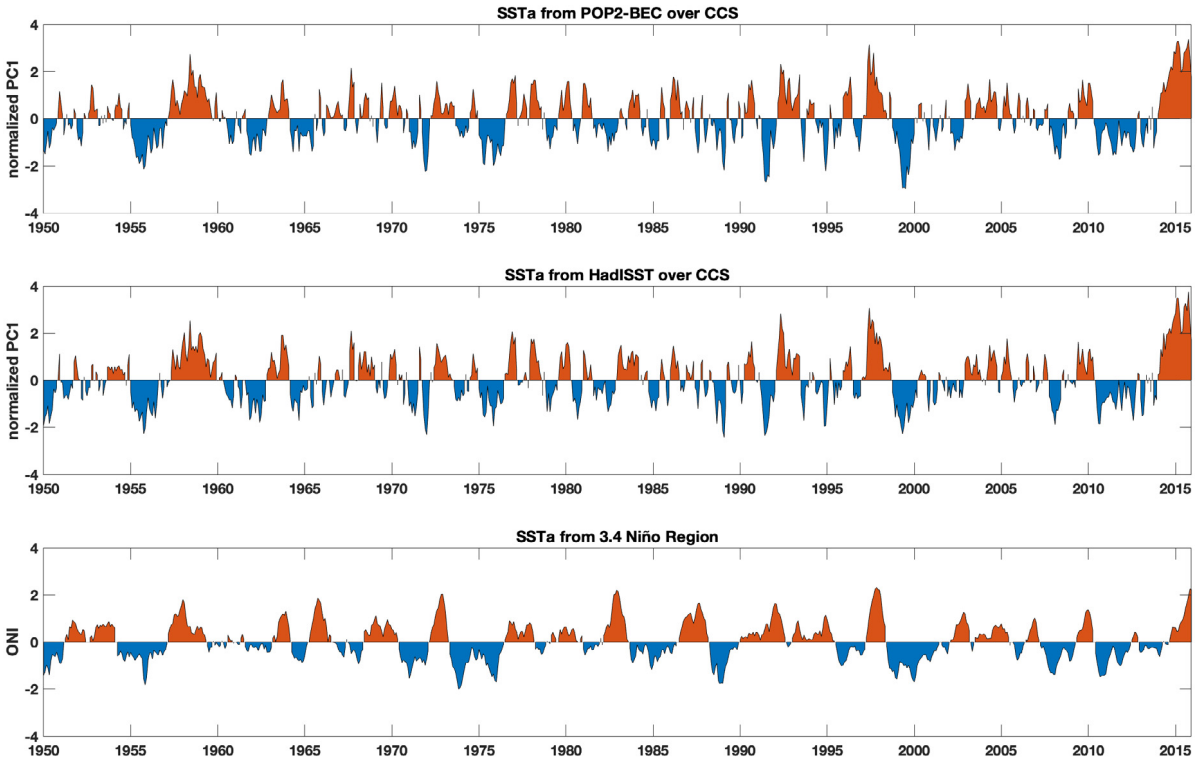

Fig. 2. Normalized principal component (PC1) associated with the first EOF of SSTa over CCS; (*top and middle*) model and observations, respectively. (*Bottom*) Monthly values of NOAA's CPC ONI is shown for comparison.

El Niño events in the CCS as indicated by the correlations of 0.70, 0.68, 0.78, respectively. The magnitude of the anomalies is also underestimated for these three major events at this location. The coarse model resolution, possible errors in surface forcing, and errors in model physical formulations limit the model performance in these pointwise evaluations.

3.2. Lagged correlations of the CCS with ENSO

In order to obtain a broad-brush view of the CCS response to ENSO in the CESM-POP2-BEC simulation, we computed the correlation of the ONI in the tropical Pacific with the physical–biological fields in the CCS at various lags (zero to 9 months). Rather than showing all the lagged-correlation results, Fig. 4 shows only the model's 3-month lagged-correlation response between observed ONI and the POP2-BEC fields (including all months) for SSTa, pycnocline depth and biogeochemistry over the CCS. The 3-month lag was chosen because it is able to simultaneously capture key aspects of both the well-developed physical response (after the winter peak of the atmospheric teleconnection forcing) and the still developing biological response in early spring. The results reveal the anticipated basic structure of warming, thermocline deepening, and decreased nutrient and plankton concentrations along the coast during El Niño events (*e.g.,* Schwing et al., 2005). As expected from previous studies (*e.g.,* Alexander et al., 2002; Turi et al., 2018), the maximum correlations of the ONI with the CCS response tend to occur at lags of several months. SSTa exhibits greatest lagged correlations over southern Baja California and Oregon, and weaker ones along the California coast, consistent with the coherency shown by EOF1 of the model SST. The pycnocline depth correlations are more confined to the coastal regions than those for SST, which extend further offshore. Correlations of the biogeochemistry (average nitrate concentration from 25 m–100 m and oxygen at 200-m depth) are closely related to those shown by the anomalies of the pycnocline depth. Correlations of 0 m–100 m vertically averaged chlorophyll and zooplankton are highest over southern Baja California but still significant up to the central California region. The chlorophyll and zooplankton responses (shown in detail below) expand northward and increase in magnitude later in spring and summer but fail to cover the coast of northern California and Oregon where significant ENSO-coherent anomalies are typically observed (*e.g.,* Thomas et al., 2009, 2012). The reasons for this discrepancy are not obvious but may be due to a combination of the errors in the physical circulation as well as to the oversimplified ecosystem formulation.

3.3. A composite physical–biological ENSO in the CCS

We next examine the response of the whole CCS during ENSO events, using spatially explicit composite anomalies of SST, pycnocline depth, 0 m–100 m vertically averaged chlorophyll, 0 m–100 m vertically averaged zooplankton biomass, 25 m–100 m vertically averaged nitrate, and oxygen at 200 m depth. Typically, warm (cold) anomalies related to El Niño (La Niña) peak during the winter (DJF) after developing during the previous fall (SON). For sake of simplicity, we show only the months in which the ENSO-related SST anomalies are typically the largest. Each of the field-map composite anomalies of SST shows September through December of the pre-peak year, and January through April of the following year corresponding to the peak and post-peak of the event. The pycnocline, chlorophyll, zooplankton biomass, $[NO_3]$, and dissolved $[O_2]$ composite anomalies are shown for January through August of the post-peak year because biological variables exhibit their largest ENSO-related signals after the spring bloom.

3.3.1. SST and pycnocline depth anomalies

The SSTa over the CCS (Fig. 5) show the evolution of the model composite El Niño during its development in the fall and maturation in the winter. The surface of the ocean starts warming during the fall (SON) of the year previous to the peak of the event (top panel) but anomalies do not become statistically significant until they reach maximum (warmer) values during FMA of the post-peak year. Only in these

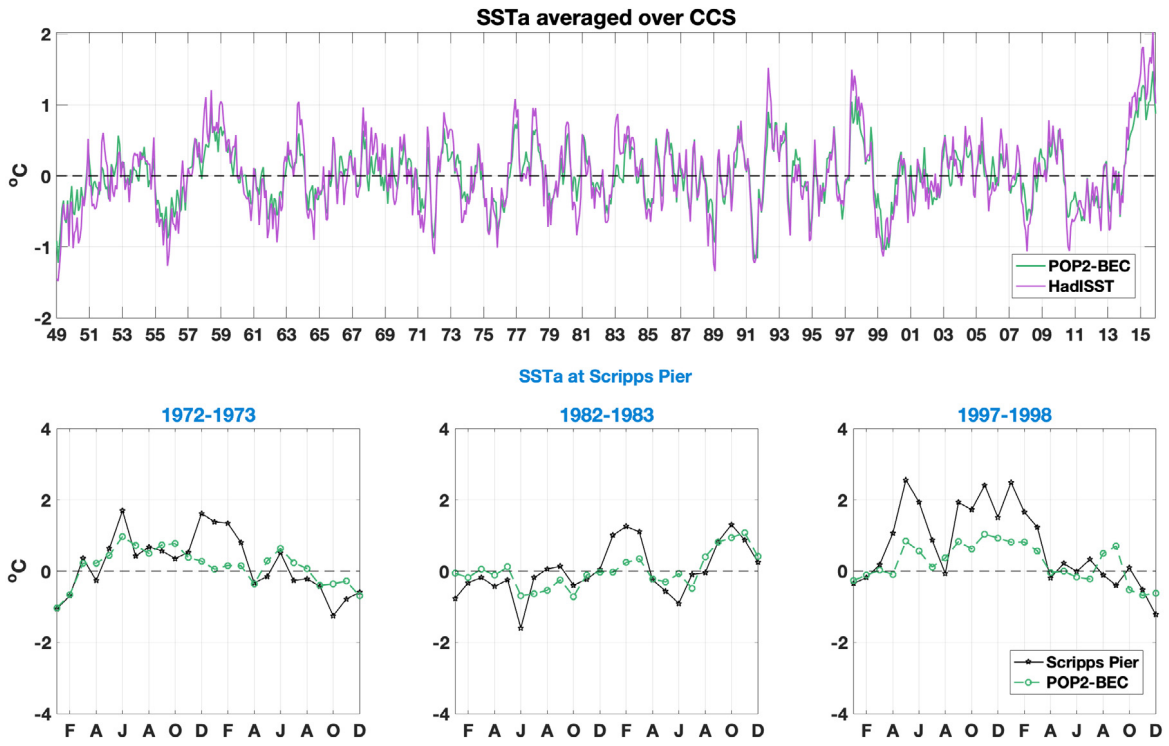

Fig. 3. (*Top*) Modeled SSTa (green) averaged over the CCS region (21–48 ˚N) and observed averaged anomalies from HadISST (purple). Correlation between the time series is 0.93 and RMS is 0.5 °C and 0.24 °C, respectively. (*Bottom*) SSTa over a single point for Scripps Pier at La Jolla CA, showing the model (green dashed line) and observations (black solid line) for three specific El Niño events as indicated by the years at the top. Respective correlations between the two time series are 0.70, 0.68, and 0.78 (left to right).

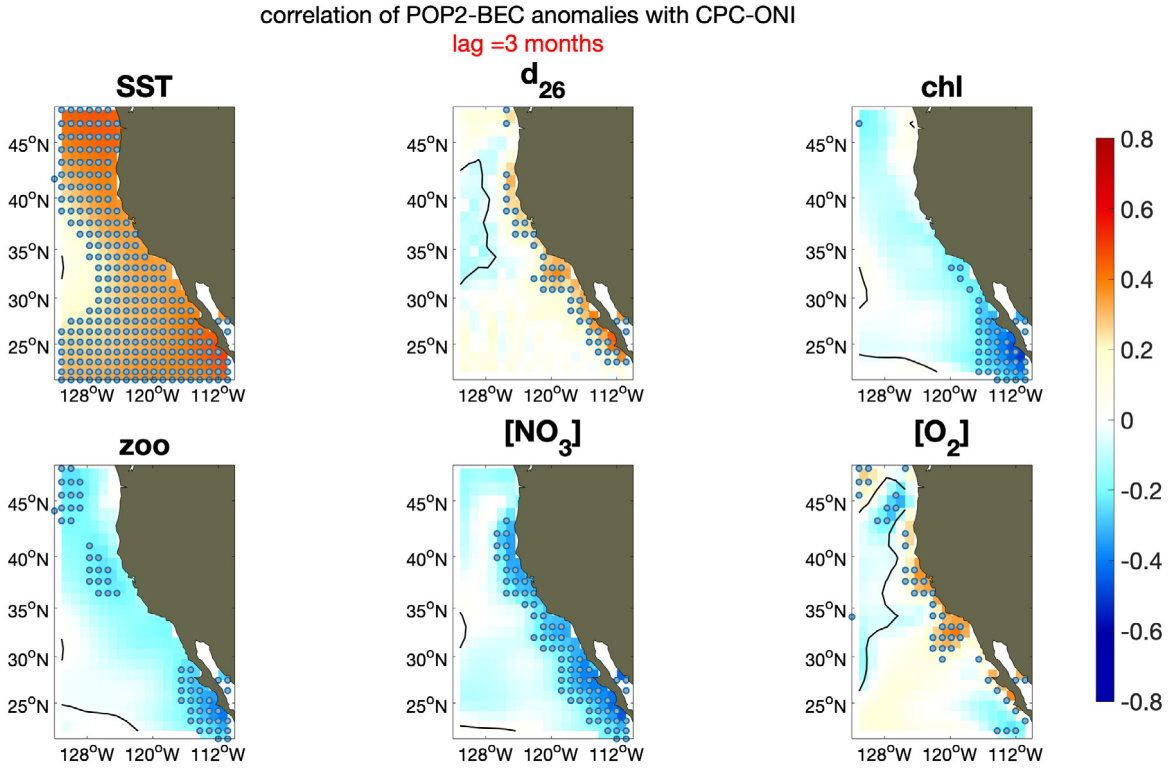

Fig. 4. Lagged (3-month) correlations of tropical Pacific ONI with modeled anomalies of SST, pycnocline depth, vertically averaged chlorophyll, zooplankton biomass, average [NO_3] over 25 m–100 m, and [O_2] at 200 m. Locations where correlations are 95% significantly greater than 0.2 are marked by gray circles.

months is the warming related to El Niño significant in the northern California Current region. In the Southern California Bight significance levels are only above 1 standard deviation from the bootstrap analysis (above 67% but below 95%, not shown). As expected from the EOF and correlation analyses, warming also occurs along Baja California, although it does not reach our level of significance. The cool SST that

develops far offshore is the eastern extent of the cold central Pacific SST that develops during El Niño due to the strengthened Aleutian Low, and is associated with the spatial pattern of the Pacific Decadal Oscillation (*e.g.,* Newman et al., 2016).

The evolution of the model composite SSTa during La Niña (Fig. 6) shows the beginning of the cold phase in late fall of the pre-peak year (top panel) with intense cold anomalies off Baja California Sur. Negative anomalies exhibit the coldest temperatures during JFM, as shown in the lower panel of Fig. 6 (post-peak year). Note how the SST anomalies related to La Niña are significant (above 2 standard deviations) over broad regions offshore and along the coast in most of the region, even during the fall preceding the peak of the cold event. In contrast to the El Niño model composite, La Niña develops earlier, more strongly, and over broader areas than El Niño, indicating that the response of the CCS is asymmetric (*e.g.,* Fiedler and Mantua, 2017). This asymmetry will be more extensively explored in later sections.

The composite evolution of observed SSTa during El Niño and La Niña events is shown in Figs. 7 and 8, respectively. Composite anomalies from the HadISST record generally show similar spatial patterns to those in the model for both warm and cold events. The magnitudes (and consequent significance) of the anomalies are generally much higher in the observations, however, especially along the coast of Baja California during the peak of warm events in DJF. We note that the observed composite anomalies also reveal more intense (and more significant) anomalies during La Niña events compared to El Niño, with the winter after the La Niña peak exhibiting a significant cooling of the whole CCS (Fig. 8). This asymmetry is consistent with what was found for the model composite in Figs. 5–6.

The pycnocline depth composite over the CCS was calculated using the $\sigma = 26$ isopycnal surface as a proxy (*e.g.,* Di Lorenzo et al., 2005; Kim and Miller, 2007). It is typically located between 180 m and 250 m in the model, while in nature the depth is often shallower, roughly 50 m to 200 m depths (*e.g.,* Rudnick et al., 2017). As anticipated from the correlation analysis, the composite El Niño anomalies for the post-peak year (Fig. 9) show a deepening of the pycnocline that starts developing during January and February along the coast, peaks during the spring, and persists into the summer season. During La Niña (Fig. 10), the reverse occurs in the composite, as a significantly shallower thermocline starts developing off the coast of Baja California during February, and the anomalies intensify during the spring and the summer. The CCS pycnocline depth response to ENSO is mainly confined to the coastal region, and at early stages is only significant at southern latitudes in the regions adjacent to the coast. This is consistent with what is observed in other studies that also report a latitudinal dependence in the response of the pycnocline (Jacox et al., 2015; Frischknecht et al., 2015), as well as in other variables such as sea-surface height and average temperature of the upper 100 m (Crawford, 2017).

A deeper pycnocline is expected over the CCS during El Niño due to the southerly wind anomalies acting to suppress upwelling as well as from remotely driven coastally trapped Kelvin-like waves (Chávez and Messié, 2009; Jacox et al., 2015; Frischknecht et al., 2015). However, the coarse resolution model cannot properly resolve this Kelvin-like wave propagation effect, so that even though the model exhibits deeper (shallower) values associated with El Niño (La Niña), the response can be muted with respect to the observed variability (*e.g.,* Hsieh, 1983). Comparing our results to the data assimilated ocean analysis study of Jacox et al. (2015) indicates that the ENSO-forced pycnocline response in CESM-POP2 is lagged by 1-to-2 months depending on the latitude along the California Coast. The anomalies of the pycnocline depth reach their peak during the spring (March–April) in the southern CCS, and after this season over northern locations. Jacox et al. (2015) also report that the timing of the ENSO-forced minimum depth of the pycnocline depends on latitude, but that it varies from March–April off central California to June–July off the Oregon coast. The mismatch with the data-assimilated product is likely due to the coarse resolution, which cannot resolve the upwelling that occurs on the Rossby deformation-radius scale that ranges from ~20 km in the northern CCS coast to ~40 km along the southern Baja California coast (*e.g.,* Chelton et al., 1998). These local coastal effects thereby become diluted into broader areas adjacent to the coast where other large-scale processes of surface-heating, advection, and open-ocean upwelling can interact with that coastally driven response.

3.3.2. Chlorophyll

Turning our attention to a biological variable, Fig. 11 shows the composite anomalies of the 0 m–100 m vertically averaged chlorophyll (including all 3 phytoplankton groups) from January to August of the post-peak year of El Niño. The structures seen in chlorophyll are less organized than for the physical variables. As anticipated from the 3-month lagged-correlation with the tropical Pacific ONI (Fig. 4), negative chlorophyll anomalies (with small amplitudes of ~1%–3% of the typical seasonal mean values) along the Baja California coast are the most consistent feature throughout the post-peak composite. They turn significantly negative during April off both Baja and central CCS, and then persist into the summer, extending further north through July and August. This response is coherent with the timing of the anomalies of the model pycnocline depth, and with its latitudinal dependence. While pycnocline anomalies show a delay with what is typically observed, chlorophyll anomalies occur within the time frame observed by previous studies (*e.g.,* Thomas et al., 2012; Kilpatrick et al., 2018). Anomalous patches of relatively high chlorophyll are shown at the Oregon coast and off-shore during January through March, but they are not significant and are likely due to errors in the interpolation of the wind forcing near the coastal boundary or errors in the model.

Fig. 12 shows the analogous evolution of the composite chlorophyll anomalies during La Niña. Late spring (April–May) and summer months during the post-peak year of the composite are dominated by the positive anomalies of chlorophyll (~1%–3% of typical seasonal mean values), showing that the model captures the enhancement of the climatological spring bloom (McGowan et al., 2003; Kim et al., 2009; Thomas et al., 2012; Goebel et al., 2010). The composite response of the CCS chlorophyll during La Niña is also coherent with the variability of the pycnocline depth and offshore SSTa, and also shows a latitudinal differentiation. Negative chlorophyll anomalies prevail off the Oregon and Washington coasts throughout this post-peak period, a result that is opposite to what observed, although not significant (*e.g.,* Fig. 7a of Thomas et al., 2012), indicating potential errors in the model or forcing fields.

Since chlorophyll is computed in the model as a nonlinear relationship involving the three phytoplankton components and other variables (*e.g.,* Moore et al., 2002), we computed composites of the biomass of diatoms, diazotrophs, and small phytoplankton separately to determine if any of them behaved more coherently in their response to ENSO variations. Both the diatoms and the small phytoplankton exhibited the same basic features seen in the chlorophyll composites. The diazotrophs, in contrast, had very small biomass compared to the other two phytoplankton and were limited spatially to offshore regions in the southern CCS domain. Therefore, the chlorophyll composites give an accurate depiction of the model's ability to represent the large-scale coherent phytoplankton biomass response to ENSO-related variations.

To further explore the model's ability to represent chlorophyll compared to nature, the CCS was divided into two sub-regions and compared to surface chlorophyll of satellite observations from SeaWiFS. Two boxes were selected: southern CCS is located between 32–38°N and northern CCS between 38–47°N, both with an approximate extension of 400 km from the coast. The model was averaged down to a depth of 25 m for comparison with the observations that sample an optical depth. Climatological values of chlorophyll from the period of 1998–2010 are shown in the left panels of Fig. 13. The model severely underestimates the mean values as indicated by the different y-axes scales. This is consistent with the analysis of Moore et al. (2004, their

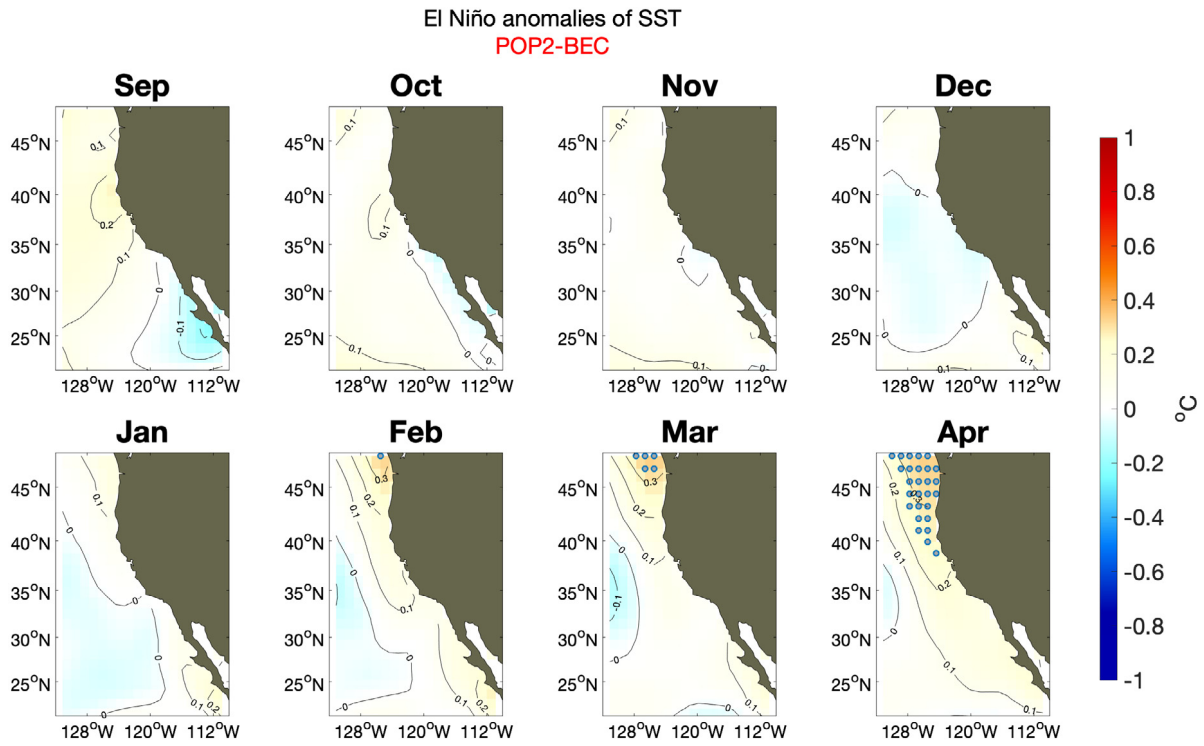

Fig. 5. Modeled composite El Niño SSTa. Significant warm (red) anomalies above the 95% confidence level are marked by gray circles . (For interpretation of the references to color in this figure legend, the reader is referred to the web version of this article.)

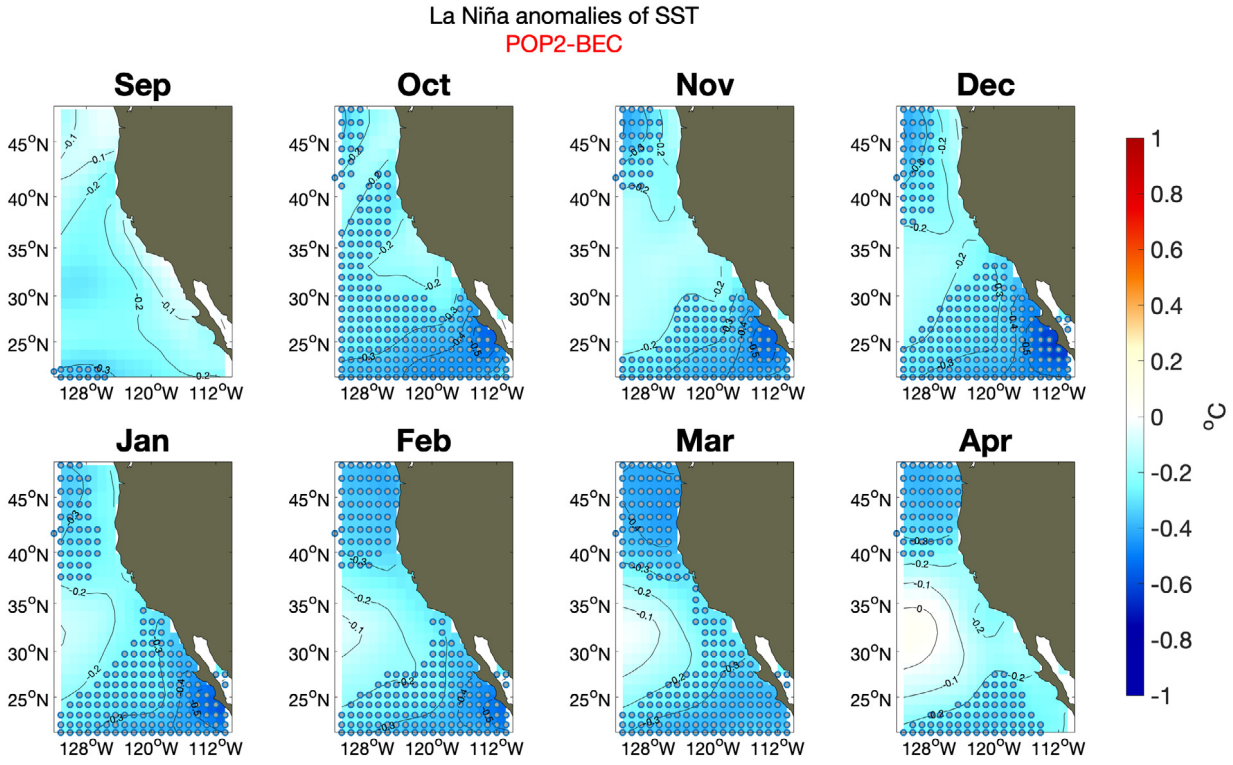

Fig. 6. Modeled composite La Niña SSTa. Significantly cold (blue) anomalies above the 95% confidence level are marked by gray circles . (For interpretation of the references to color in this figure legend, the reader is referred to the web version of this article.)

Fig. 3) who showed very weak mean springtime chlorophyll in the CCS region for BEC compared to other areas where the model compared better with satellite observations. Both the climatological values and the anomalies are one order of magnitude smaller than in observations. The seasonal timing of the modeled mean chlorophyll is generally consistent with the observations in the northern part of CCS. Both peak during wintertime (DJF) and early spring (MA), and consistently decrease during summertime (JJA). The modeled variability in the southern CCS shows some differences compared to the observed timing, particularly during the summer months (JJA) where the modeled

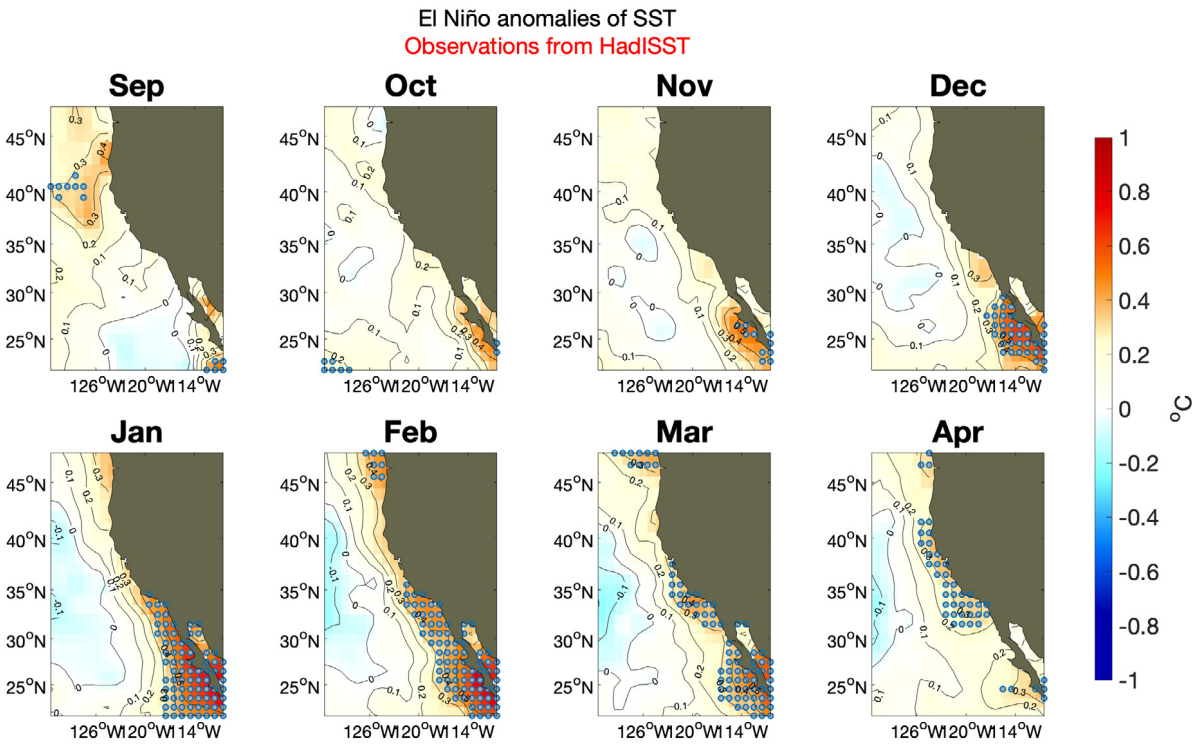

Fig. 7. Observed (HadISST) composite SSTa from 13 El Niño events in the period from 1949–2015. Significant warm (red) anomalies above the 95% confidence level are marked by gray circles . (For interpretation of the references to color in this figure legend, the reader is referred to the web version of this article.)

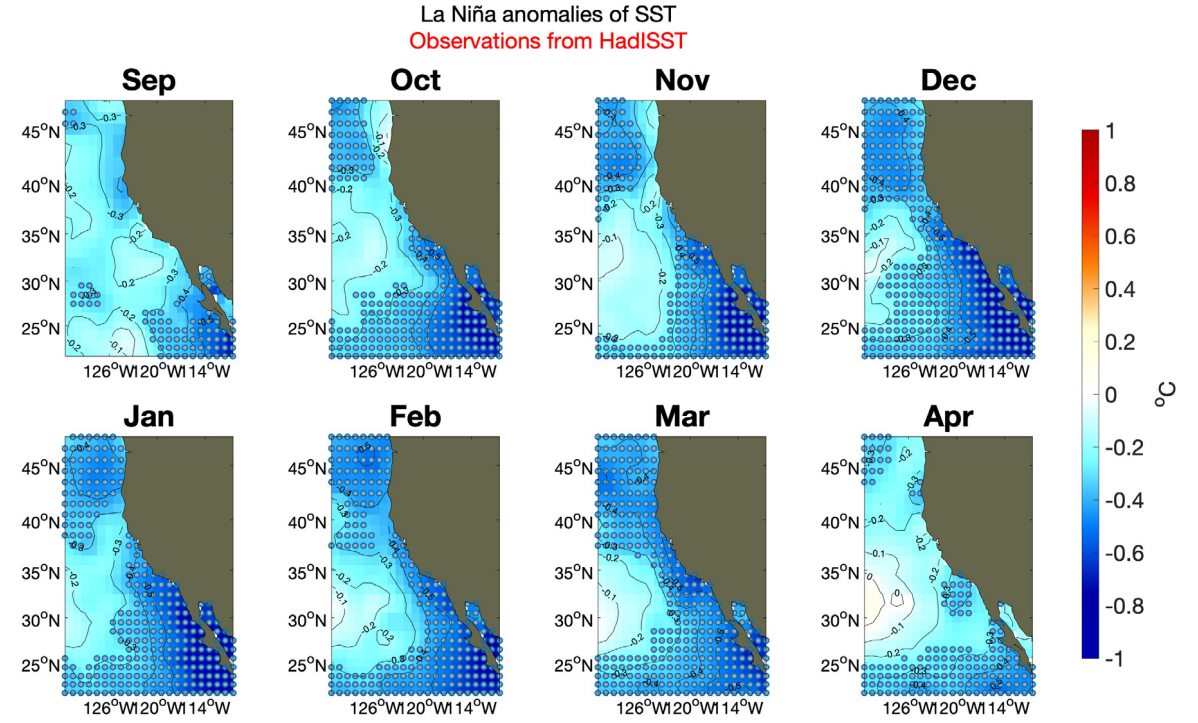

Fig. 8. Observed (HadISST) composite SSTa from 13 La Niña events in the period from 1949–2015. Significantly cold (blue) anomalies above the 95% confidence level are marked by gray circles.

values drop down but the observed chlorophyll persists from winter through August. Surface chlorophyll anomalies from the model in the CCS are in poor agreement with the satellite surface observations over the 1998–2010 time period as indicated by the small and insignificant correlations in both the north and south CCS regions when including all months (i.e., for El Niño, La Niña, and neutral conditions together). This is in contrast to the composites that reveal coherent signals (although very small) associated with the warm and cold ENSO events.

3.3.3. *Nutrients and dissolved oxygen*

The model composite evolution of [NO_3] anomalies during El Niño is shown in Fig. 14. In contrast with the chlorophyll response that

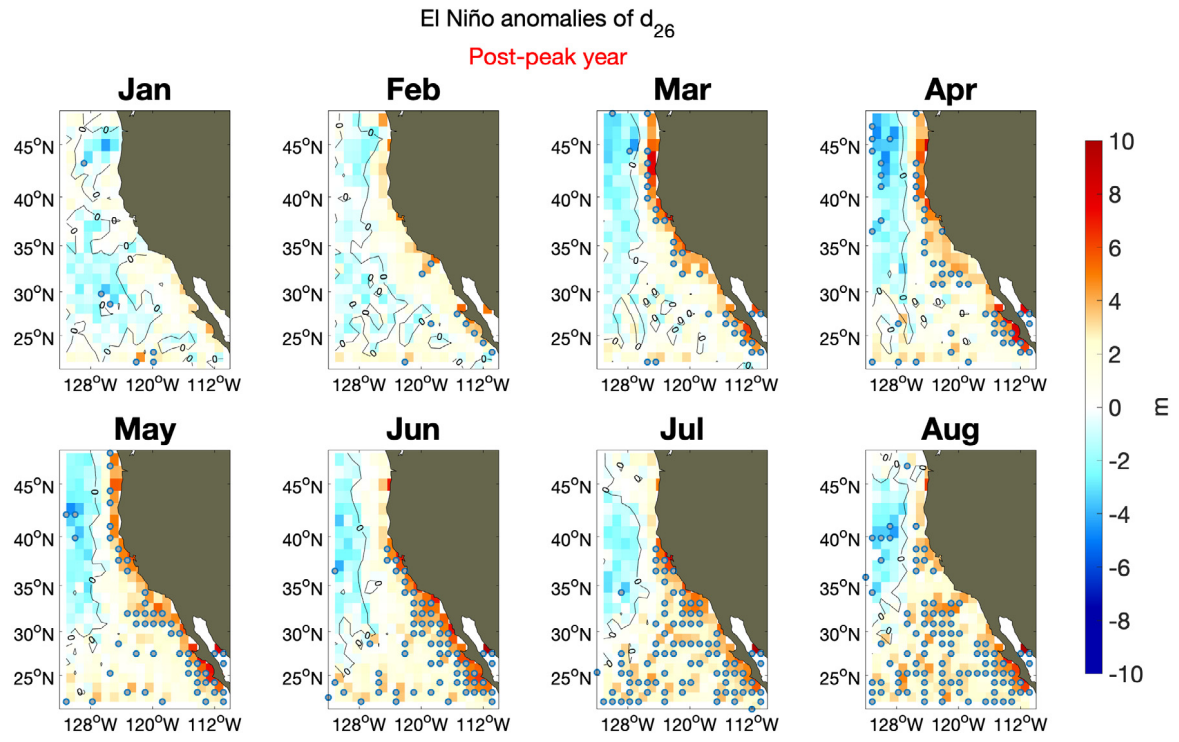

Fig. 9. Modeled composite El Niño pycnocline depth anomalies, (d26). Significantly deep (red) anomalies above the 95% confidence level are marked by gray circles.

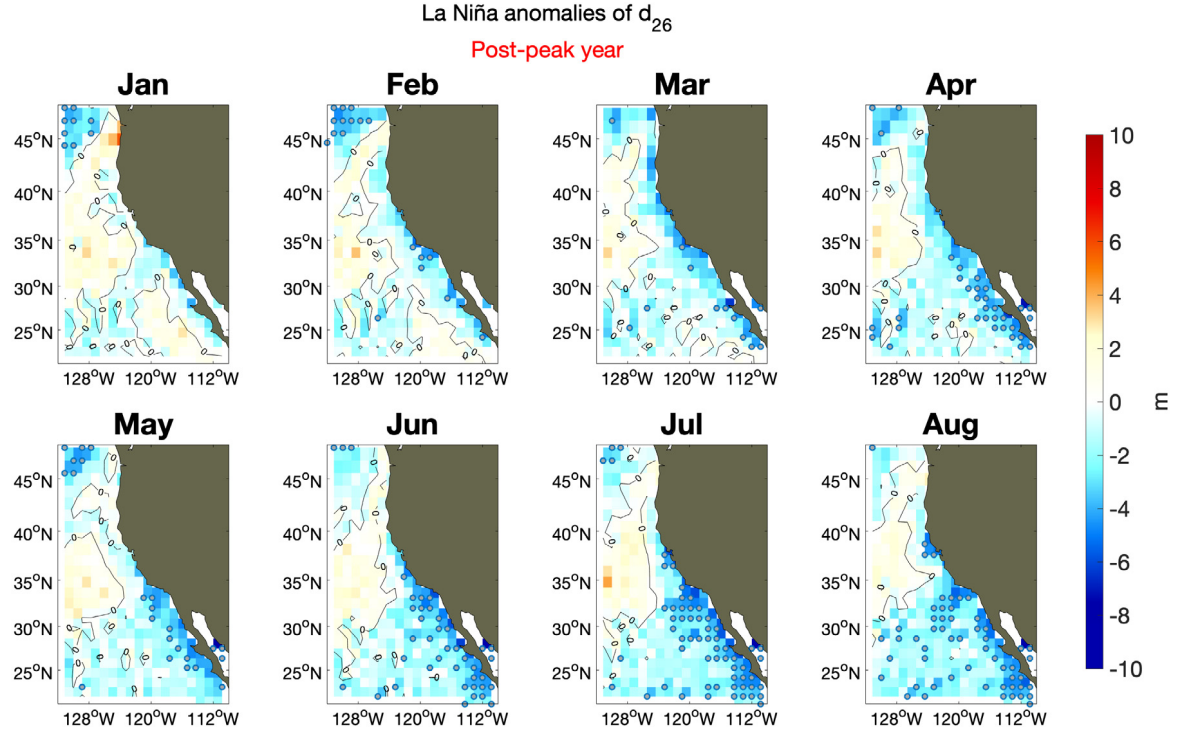

Fig. 10. Modeled composite La Niña pycnocline depth anomalies, (d26). Significantly shallower (blue) anomalies above the 95% confidence level are marked by gray circles.

shows marked differences with latitude, nitrate concentrations seem to respond uniformly along the CCS during the spring, when negative anomalies associated with El Niño reach their maximum in the model. This variability is very coherent with the timing shown by the anomalies of the pycnocline depth, as would be expected from the results of the correlation analysis. Depleted nutrient concentrations during El Niño are consistent with the typically downwelling-favorable anomalous wind fields (*e.g.*, Jacox et al., 2017), consequent deepening of the pycnocline, and muted upwelling of source waters. The opposite situation occurs during La Niña (Fig. 15), when intensified upwelling favors higher [NO_3] that starts to show as early as February in the southern CCS and peaks during the spring over the whole CCS. Both El Niño and La Niña composites show anomalies that persist through the summer, consistent with chlorophyll anomalies. The magnitude of

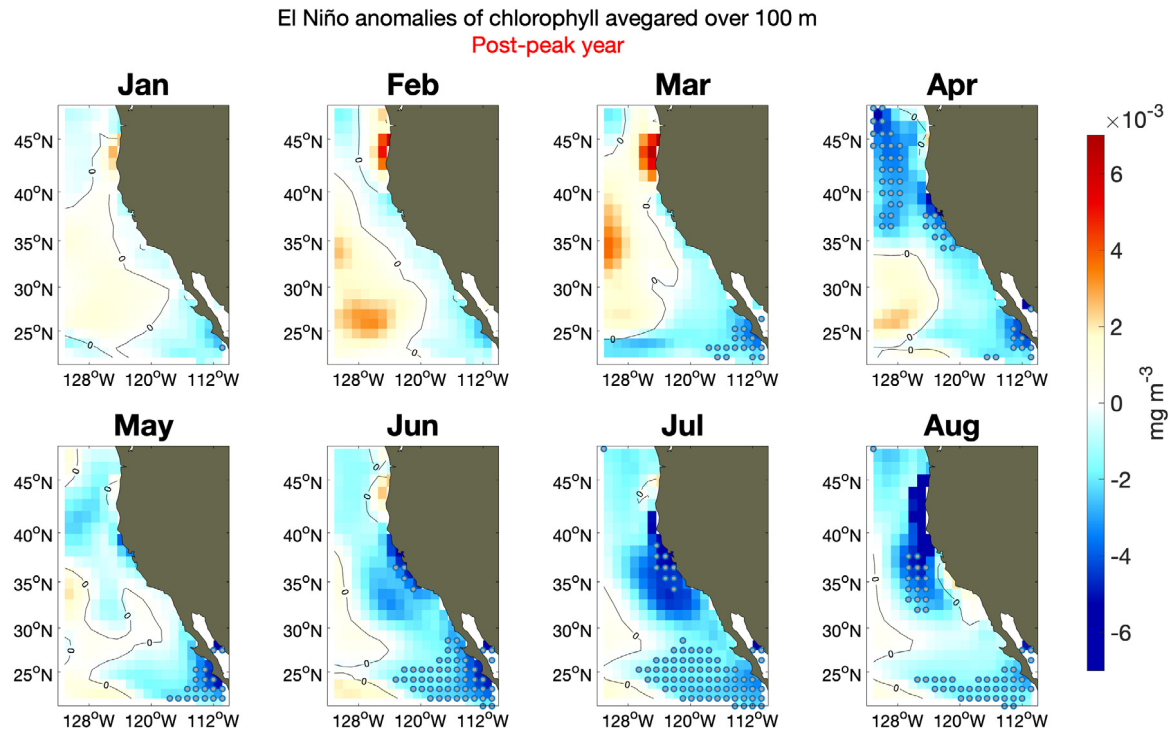

Fig. 11. Modeled post-peak El Niño composite vertically averaged (down to 100 m) chlorophyll anomalies. Significantly lower chlorophyll anomalies (blue) are marked by gray circles.

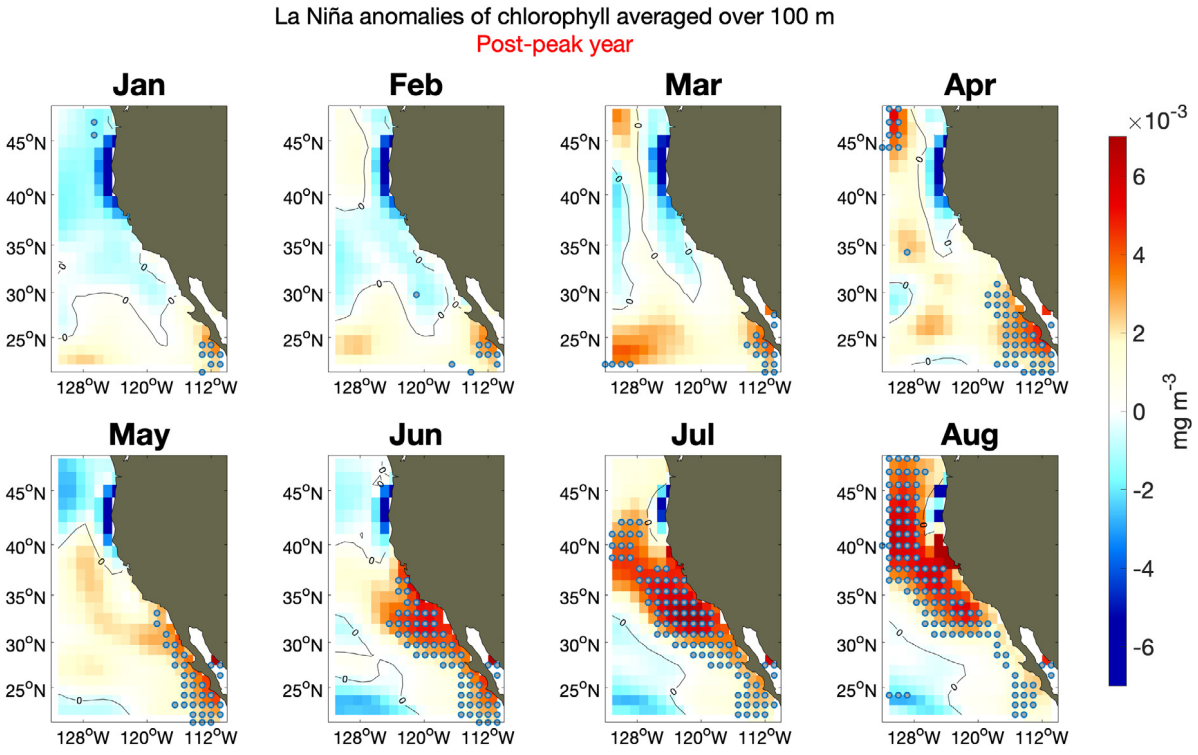

Fig. 12. Modeled post-peak La Niña composite vertically averaged (surface to 100 m). Significantly higher chlorophyll anomalies (red) are marked by gray circles.

these nitrate anomalies, ~0.5 mmol m^{-3}, is rather small compared to typical mean values of 20 mmol m^{-3}. But this is to be expected for monthly mean anomalies because of the rapid response time (~days) of phytoplankton in the euphotic zone that results in an equilibrated balance between vertical nutrient flux, uptake by phytoplankton, and grazing by zooplankton.

Composite dissolved oxygen concentrations at 200 m show patterns similar to the nutrient composites. During El Niño events the pycnocline is depressed, which then acts to push down the oxygen minimum zone in the areas adjacent to the coast, resulting in relatively higher dissolved [O_2] at 200 m (Fig. 16). The opposite situation occurs during La Niña events (Fig. 17), when upwelling of isopycnal surfaces shifts

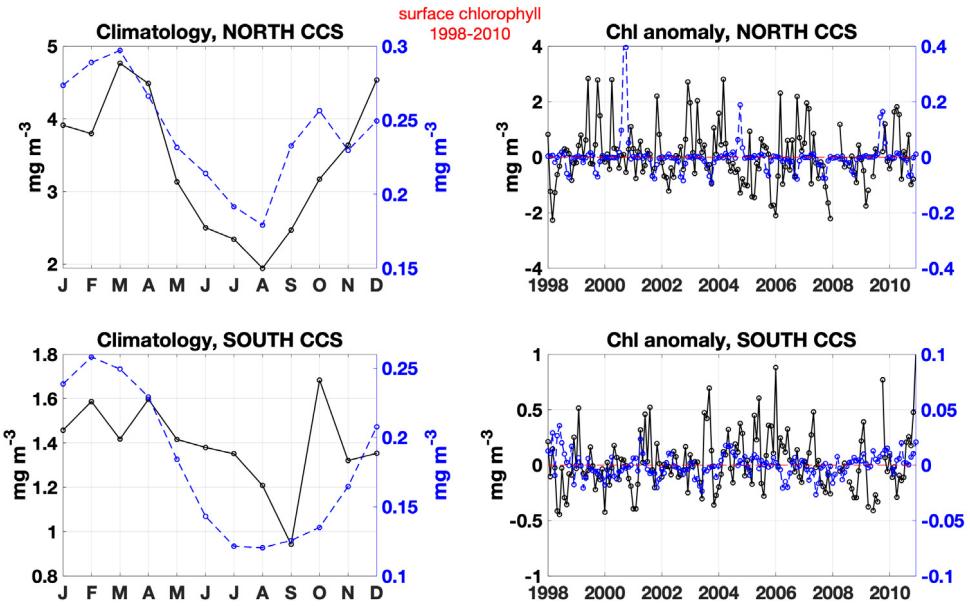

Fig. 13. Comparison of (vertically averaged, surfaceto 25 m) chlorophyll from BEC (blue) with SeaWiFS (black) for North CCS (38–47°N) and South CCS (32–38°N). Climatological values are shown in the left panels and the right panels represent the anomaly time series for the period 1998–2010 . (For interpretation of the references to color in this figure legend, the reader is referred to the web version of this article.)

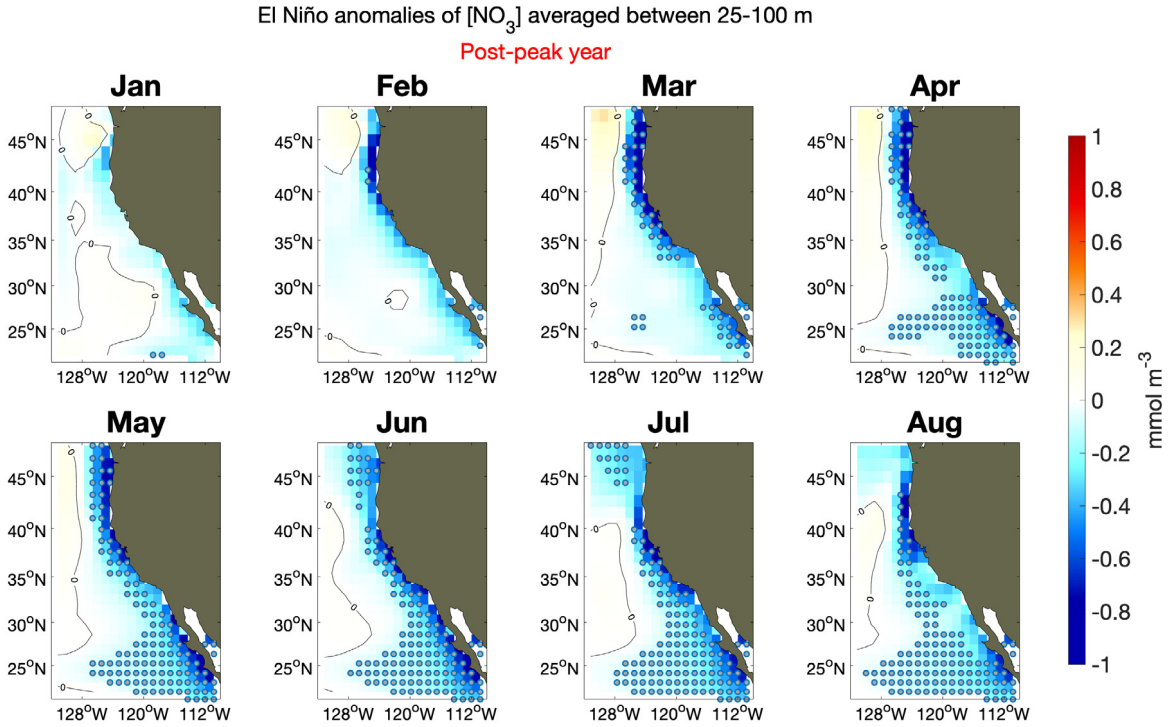

Fig. 14. Modeled post-peak El Niño composite of [NO_3] averaged between 25 m to 100 m. Significantly lower anomalies (blue) are marked by gray circles.

the level of minimum oxygen to shallower depths, and dissolved [O_2] is depleted ~3–5 mmol m^{-3} relative to normal conditions (~50 mmol m^{-3}) at 200 m. (The model composites also reveal oxygen anomalies of reversed sign off the coast of Washington, although they tend to lack statistical significance.) Our results are consistent with those shown by Turi et al. (2018), where their composites of oxygen at 100 m reveal an increase in dissolved [O_2] during warm events. The response shown by their results is also confined to a coastal band that extends ~200 km offshore, while most of the deeper ocean shows little response to El Niño.

We emphasize that the composite variability of dissolved oxygen and nutrients represented by the model is limited by the coarse resolution to include only large-scale processes and parameterized eddy-mixing effects. This results in a relatively simple link between the large-scale changes imprinted by the ENSO and the direct effects on nutrients and [O_2] that are mainly determined by changes in the thermocline depth. Unresolved mesoscale and submesoscale processes that contribute to lateral and vertical mixing can also play a different and very important role in altering these patterns (*e.g.,* Gruber et al., 2011; Di Lorenzo et al., 2013; Jacox et al., 2015; Frischknecht et al., 2018), which should be explored in additional work.

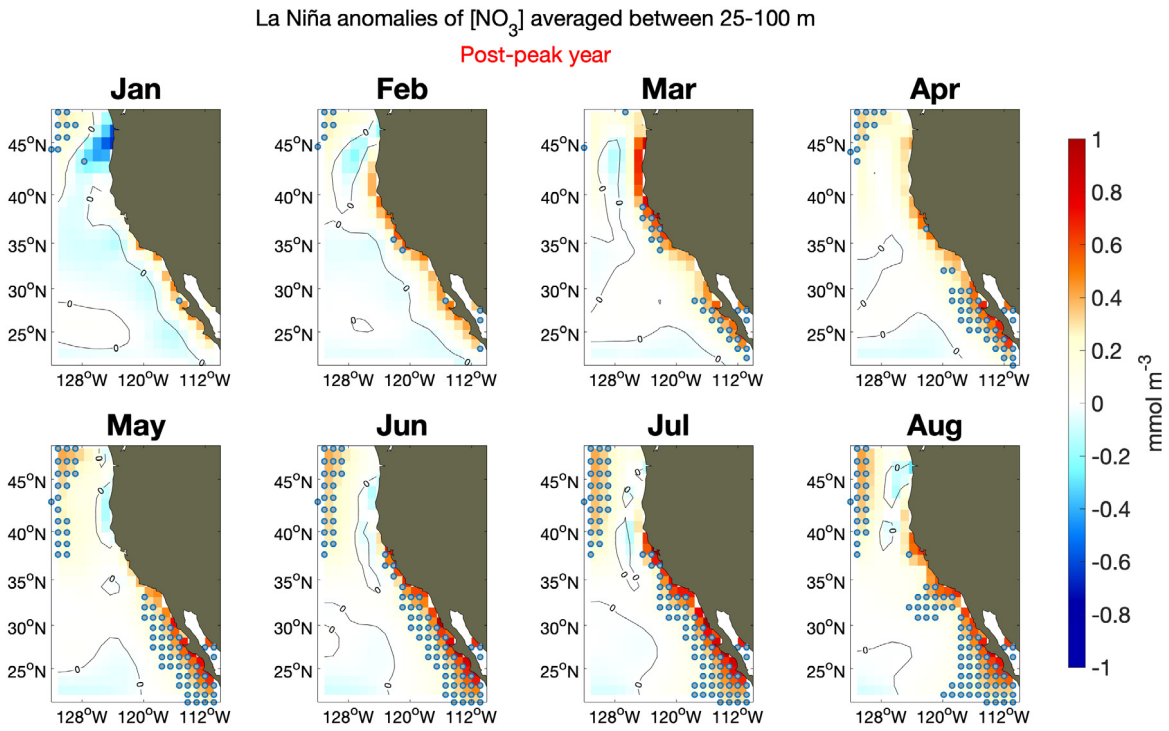

Fig. 15. Modeled post-peak La Niña composite of [NO_3] averaged between 25 m to 100 m. Significantly higher anomalies (red) are marked by gray circles.

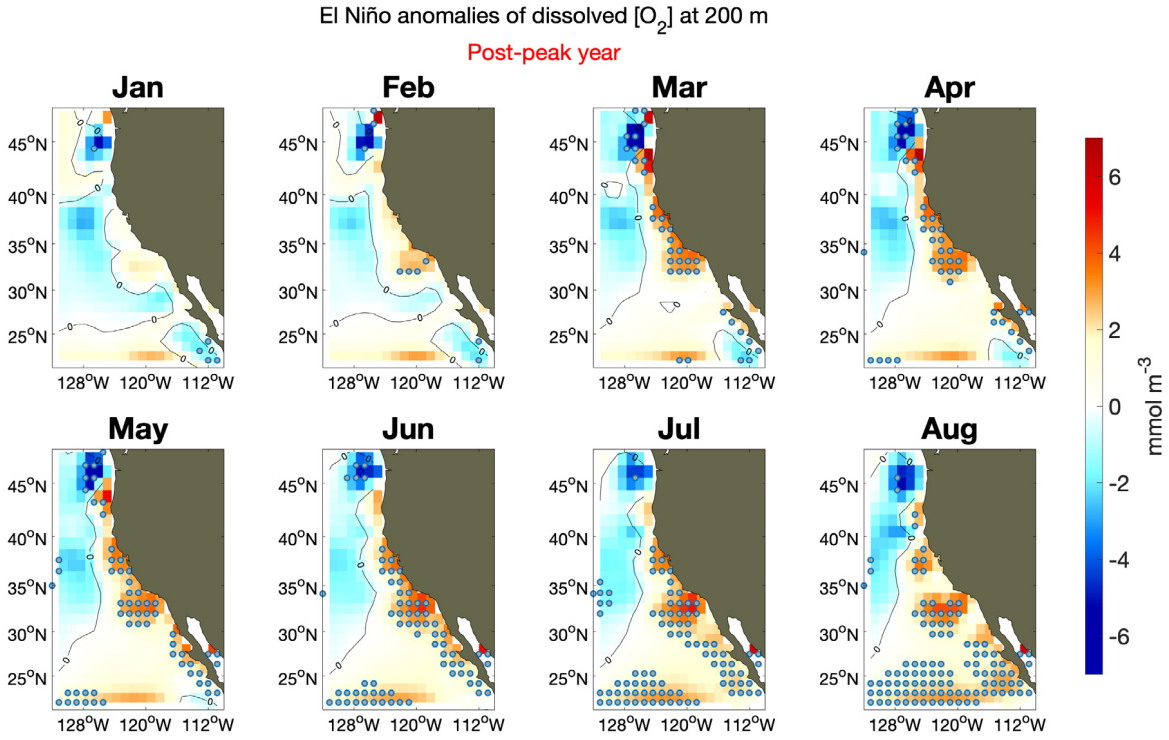

Fig. 16. Modeled post-peak El Niño composite [O_2] at 200 m depth. Significantly higher values (red) are marked by gray circles.

3.3.4. Zooplankton

Fig. 18 represents the composite evolution of the post-peak year of El Niño for the zooplankton group in the model. The response resembles the one shown by the chlorophyll anomalies (see Fig. 11), with negative values that are well developed by summer (JJA), but are weaker in winter and early spring. The modeled zooplankton also exhibits a stronger (and more significant) response during La Niña (Fig. 19) compared to the composite El Niño, and positive blooms begin off the coast of Baja California during Jan–Feb, persisting through the spring and extending further north in the CCS in the summer. The magnitude of the zooplankton anomalies coherent with ENSO in the model is a few percent of the mean background state.

While some previous studies have shown a rather direct link between ENSO conditions and zooplankton (*e.g.,* Bograd and Lynn, 2001; Fisher et al., 2015), one recent study on samples from CalCOFI cruises suggests that changes in zooplankton community can only be related

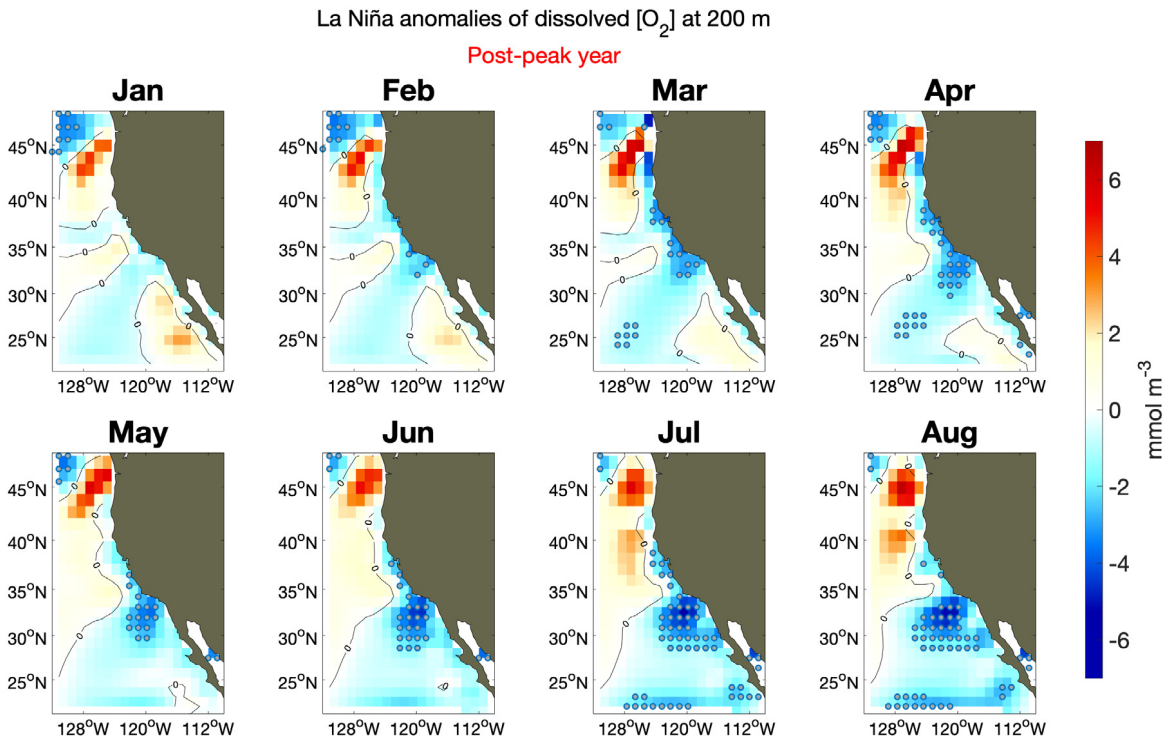

Fig. 17. Modeled post-peak La Niña composite [O_2] at 200 m depth. Significantly lower values (blue) are marked by gray circles.

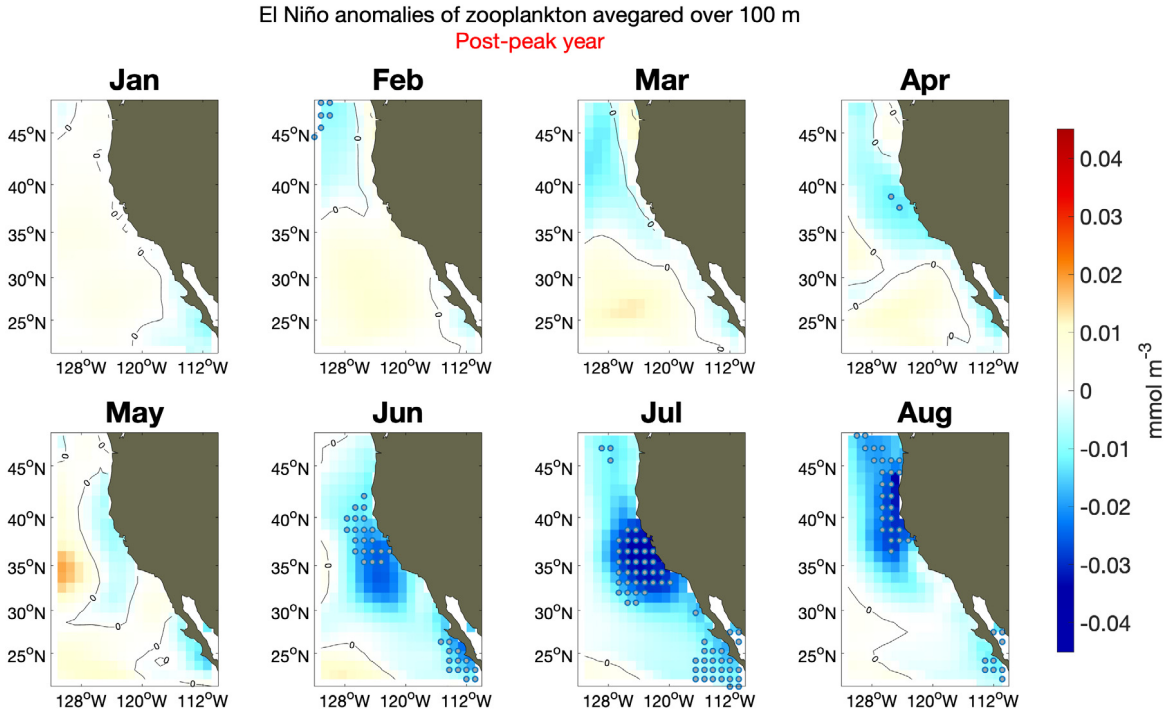

Fig. 18. Modeled post-peak El Niño composite vertically averaged (surface to 100 m) zooplankton biomass anomalies. Significantly lower anomalies (blue) are marked by gray circles.

to El Niño at the level of species and individual taxonomic groups. Although some taxa, such as euphausiids and calanoid copepods, showed a decline in biomass during El Niños 1958, 1959, 1983, 1992, 1993, 1998, 2003, 2010, and 2016, total mesozooplankton biomass does not vary consistently (Lilly and Ohman, 2018). The same study reports that some of the species of copepods and euphausiids actually decreased in biomass during la Niña (for years 1951, 1956, 1965, 1989, 1999, 2000, and 2008).

The zooplankton included in the model is a simplified formulation as an aggregate group that includes microzooplankton and mesozooplankton with no representation of a particular group. The response of the CCS shown by the composite anomalies seems to be very well defined as negative values during El Niño and positive during La Niña,

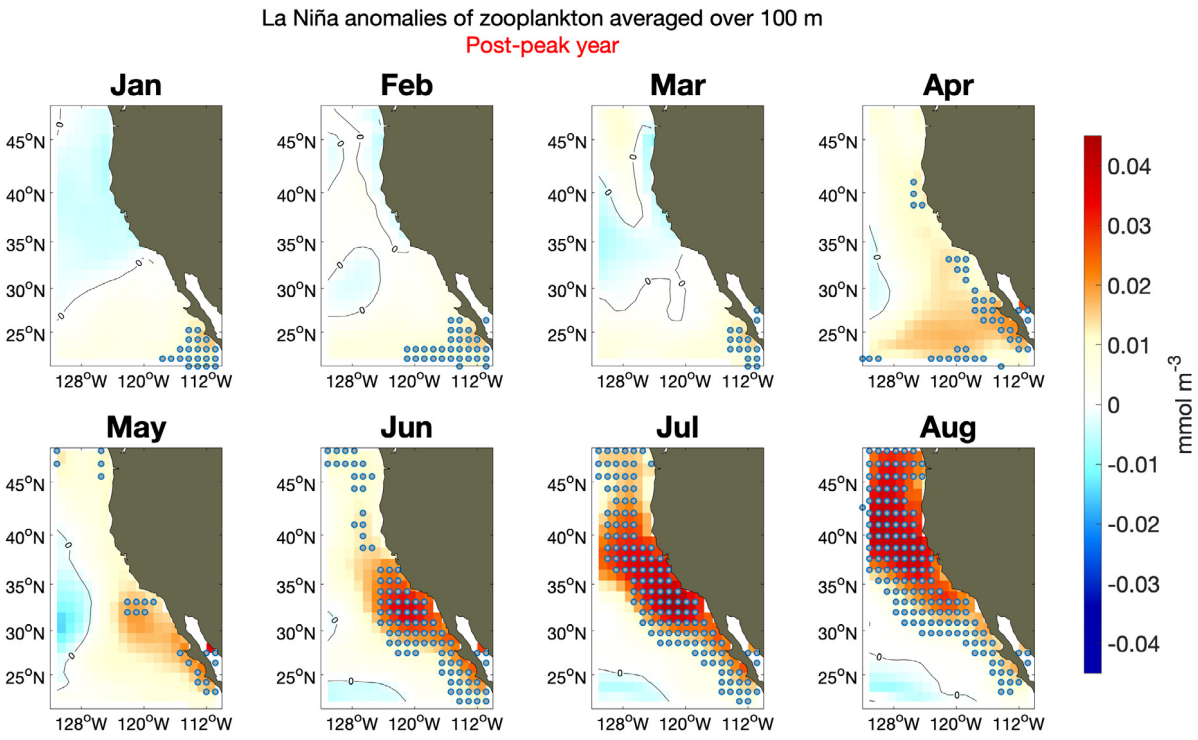

Fig. 19. Modeled post-peak La Niña composite vertically averaged (surface to 100 m) zooplankton biomass anomalies. Significantly higher anomalies (red) are marked by gray circles.

with a strong correlation to model phytoplankton, while observations indicate that zooplankton community is not consistently affected during warm versus cold ENSO events.

4. Discussion

A physical–biological ocean model hindcast of the time period 1949–2015 was analyzed to establish its skill levels on interannual timescales when compared with available observations and to construct composite El Niño and La Niña events for the California Current System. We found that when averaging the model response over the entire CCS, it well reproduces the SSTa estimated from HadISST. When considering smaller regional averages or individual points (such as Scripps Pier), the model exhibits less coherency with SST observations and tends to have a lower amplitude. Much of this disagreement can be ascribed to the coarse resolution (~1°) of the simulation, but issues associated with errors in the surface forcing functions may also be involved. For example, the interpolation scheme for the winds incorporates winds over land for oceanic grid points adjacent to the coast, which can adversely affect the coastal upwelling and offshore wind-stress curl fields that provide the dominant forcing of the coastal ocean.

There are many approaches to identify the effects of ENSO over the CCS. For instance, one could treat each ENSO event individually as has been done previously in many case studies (*e.g.,* Bograd and Lynn, 2001; Frischknecht et al., 2017), which corresponds to the extreme view that each ENSO event is totally different from other events due to differing tropical teleconnections or to random variability of the midlatitude weather systems (e.g., Deser et al., 2018; Capotondi et al., 2019). But the composite approach is useful to provide a picture of the consistent types of responses that would be expected to be found for a typical event. One could alternatively also separate the warm and cold events into finer-grained samples, *e.g.,* associated with Central Pacific vs. Eastern Pacific events (*e.g.,* Ashok et al., 2007; Di Lorenzo et al., 2010; Capotondi et al., 2019), or perhaps using some other criterion to create even more groups of warmish or coldish events. However, as Capotondi et al. (2015) clearly state, there is no strict bimodality evident in the ENSO distribution, which may be more properly defined as a continuum. Among the many different ways to address the topic, we chose a composite approach using 14 warm and 15 cold, moderate-to-large events to give a general view of the CCS response in the CESM-POP2-BEC simulation.

The maps of model ENSO composite anomalies exhibit their strongest signals in the post-peak winter and spring for SST and pycnocline depth, and in the post-peak winter through summer for chlorophyll, zooplankton biomass, [NO_3], and dissolved [O_2]. While SST responds relatively uniformly over the whole north-south region of the CCS during model ENSO events, the response of the pycnocline depth and the biogeochemistry shows a latitudinal dependence that was also noted in previous studies using observations and models (Chenillat et al., 2012; Jacox et al., 2015; Crawford et al., 2017). Oxygen at 200 m is controlled in the model mainly by the physical forcing associated with changes in upwelling and downwelling, but we did not explore potential influences of horizontal ocean currents or changes in oxygen solubility.

The response of the ENSO composite pycnocline depth in the model is delayed by a period of 1 to 2 months compared to observations (*e.g.,* Lynn and Simpson, 1987; Collins et al., 2003; Jacox et al., 2015). More recently, Crawford (2017) used a multivariate EOF analysis of an ocean data assimilation product to show that peak anomalies of the pycnocline depth occur during February over the CCS, which is 1-to-2 months earlier than we found here. While further study is necessary to explain this delayed isopycnal response in POP2-BEC, we can speculate about some of the possible mechanisms that may lead to this delay. The ocean component of the model is forced by observed winds from reanalysis, clearly accounting for the local changes in the pycnocline depth induced by the variability of the local wind stress along the California Coast. Yet the model coarse resolution will suppress (*e.g.,* Hsieh, 1983) the remotely forced variability of coastal-trapped Kelvin-like waves propagating northward along the coast that affect the pycnocline (*e.g.,* Frischknecht et al., 2015). Additionally, the coarse resolution spreads the impact of nearshore wind stress over a broader area, thereby reducing the strength of both coastal upwelling

and wind-stress-curl forced upwelling along an eastern boundary (Song et al., 2011; Small et al., 2015). These various effects may contribute to the delay in upwelling timing but additional work is required to identify the processes that can be improved in the model and should be addressed in future research.

The composite results for the model biological and chemical variables are dependent on the quality of the physical drivers. Even with the noted deficiencies of the physical state during ENSO events, coherent signatures of the ecology and biogeochemistry appear in the model composites. These variables tend to exhibit their most significant response in conjunction with the model's most consistent pycnocline response, which tends to be post-peak winter through summer for the ENSO events. This important link between the pycnocline and the modeled ecological response should be further explored in future modeling studies that include much higher resolution in the regional ocean (Curchitser et al., 2013; Frischknecht et al., 2015, 2017; Jacox et al., 2015).

The model composite CCS anomalies during El Niño and La Niña events reveal an asymmetry in that a stronger and more statistically significant La Niña influence on SSTa occurs compared to the El Niño influence, as previously discussed by Fiedler and Mantua (2017) for observations. This asymmetry also occurs prominently in the vertically averaged chlorophyll and zooplankton composite anomalies, but is less evident in the isopycnal, nitrate and oxygen fields. This cold-event asymmetry in the CCS is somewhat unexpected, since typically El Niño events exhibit a stronger SSTa in the eastern tropical Pacific than La Niña (Rodgers et al., 2004; An and Jin, 2004; Levine et al., 2016; Burgers and Stephenson, 1999), an aspect related to ENSO nonlinearities (Rodgers et al., 2004). To further explore this asymmetry, Fig. 20 shows the histograms of modeled (left) and observed (right) monthly-mean SSTa averaged along the coastal region of the CCS for months corresponding to neutral (top), El Niño (middle), and La Niña (bottom) events. The distributions reveal the tendency of the model to produce weaker variability than observations, for both neutral years and ENSO events. For both model and observations, the SSTa events in the CCS that are associated with La Niña cluster more consistently around negative values (as also discussed by Fiedler and Mantua, 2017, and seen in Fig. 5g of Turi et al., 2018), indicating the mean of the distribution shifting below zero. In contrast, both modeled and observed CCS SSTa associated with El Niño events, although they include the most extreme warming conditions (*e.g.,* McGowan et al., 1998), are often cool or only very weakly warm, and are more symmetrically distributed around zero anomaly. This results in a mean model El Niño composite response that is weaker, and less significant, than for model La Niña events. Our observed composites from the HadISST also reveal that the asymmetric response favoring La Niña is not an artifact of the model. This asymmetry is also clearly evident in the ordination diagram of Fiedler and Mantua (2017) and the mean composite warm and cold events plotted in Fig. 5g of Turi et al. (2018).

To further study the mechanism behind this asymmetric response, we examined whether the asymmetry arises in the tropical Pacific or is locally generated by the CCS winds. Fig. 21 (top) shows histograms of the observed SST anomalies in the central tropical Pacific Niño-4 region, where the teleconnections to the PNA pattern are more likely to originate through changes in deep convection (*e.g.,* Barsugli and Sardeshmukh, 2002; Alexander et al., 2002). The figure shows that the Niño-4 SST anomalies for La Niña are in fact more consistently cold than El Niño conditions are consistently warm. This tropical asymmetry has also been discussed in previous studies (*e.g.,* Dommenget et al., 2013; Cai et al., 2018). This result suggests that the teleconnections during La Niña would more consistently drive cold conditions in the CCS than would El Niño events drive warm conditions, as found in our model response and in observations. This view is further substantiated by inspecting the histograms of meridional winds averaged over the CCS, shown in Fig. 21 (bottom). As anticipated from the observed tropical Pacific Niño-4 SST asymmetry, the local winds are also more consistently upwelling favorable during La Niña conditions and less consistently downwelling favorable during El Niño conditions.

Despite the model producing very weak chlorophyll values that are poorly correlated with the time-limited monthly-mean satellite surface observations, the model shows some skill in reproducing the timing of the climatology and the model better represents seasonal chlorophyll variability in the northern region compared to the south. In contrast, the El Niño and La Niña composite vertically averaged chlorophyll response is more realistic in the southern parts of the CCS (cf. Thomas et al., 2012). Composite zooplankton anomalies are essentially phase-locked to the chlorophyll field, upon which the zooplankton graze. This linear relationship is not surprising since the model only has one zooplankton group encompassing both microzooplankton and mesozooplankton, and so cannot represent the variety of populations in the CCS. Since the response of zooplankton to ENSO events varies by taxonomic group (Lilly and Ohman, 2018), increased complexity in the modeled zooplankton is necessary to better represent zooplankton response to ENSO in the CCS. Improvements to marine ecosystem formulations via explicit representation of coastal species (*e.g.* Van Oostende et al., 2018) as well as interannually varying nutrient inputs (*e.g.,* surface runoff in the northern CCS, Hickey and Banas, 2008) could significantly improve the biogeochemical model skill in a forced ocean simulation. These types of model reformulations should be explored in future studies.

5. Conclusion

We show the composite variability of key physical and biogeochemical variables in the California Current System in the framework of the CESM-POP2-BEC model to develop a better understanding of the effects of ENSO on the oceanic ecosystem in that model. The 67-year long coarse-resolution ocean model simulation used for this study captures many of the expected main features related to ENSO events. The physical and biogeochemical processes in the simulation provide a comprehensive depiction of behavior of the system that cannot be obtained from observations alone. The simplicity of the composite approach makes it useful for determining the physical changes driven by ENSO and ascertaining how these changes affect the ecological and biogeochemical state of the model system.

The results also give a measure of the predictable nature of the model system to forcing by ENSO. As the teleconnected response to remote ENSO events impacts the local oceanography of the CCS, the fidelity of predictions is reduced not only by deficiencies in the model but by local unpredictable processes in both the physics and biology as well. The coarse resolution model had significant errors in the physical response to forcing, which then cascaded into errors in the forcing that is provided to the ecosystem model. Higher-resolution physical–biogeochemical models will help to alleviate some of the model errors, but intrinsic variability in both physics and the ecosystem will further reduce the skill of linking ENSO variations to local physical–biological response. Quantification of these types of skill limits is the long-term goal of our research. These physical–biological composites provide a view of some of the limitations to the potentially predictable impacts of ENSO on the CCS in the framework of CESM-POP2-BEC.

Acknowledgments

This study forms a portion of the Ph.D. dissertation of NCQ, who was partially supported by a UC Mexus CONACYT Fellowship. The National Science Foundation (California Current Ecosystem-LTER, OCE1637632) and the National Oceanic and Atmospheric Administration (NOAA-MAPP; NA17OAR4310106) provided additional funding for this research. Many of the ideas pursued in this study were motivated by

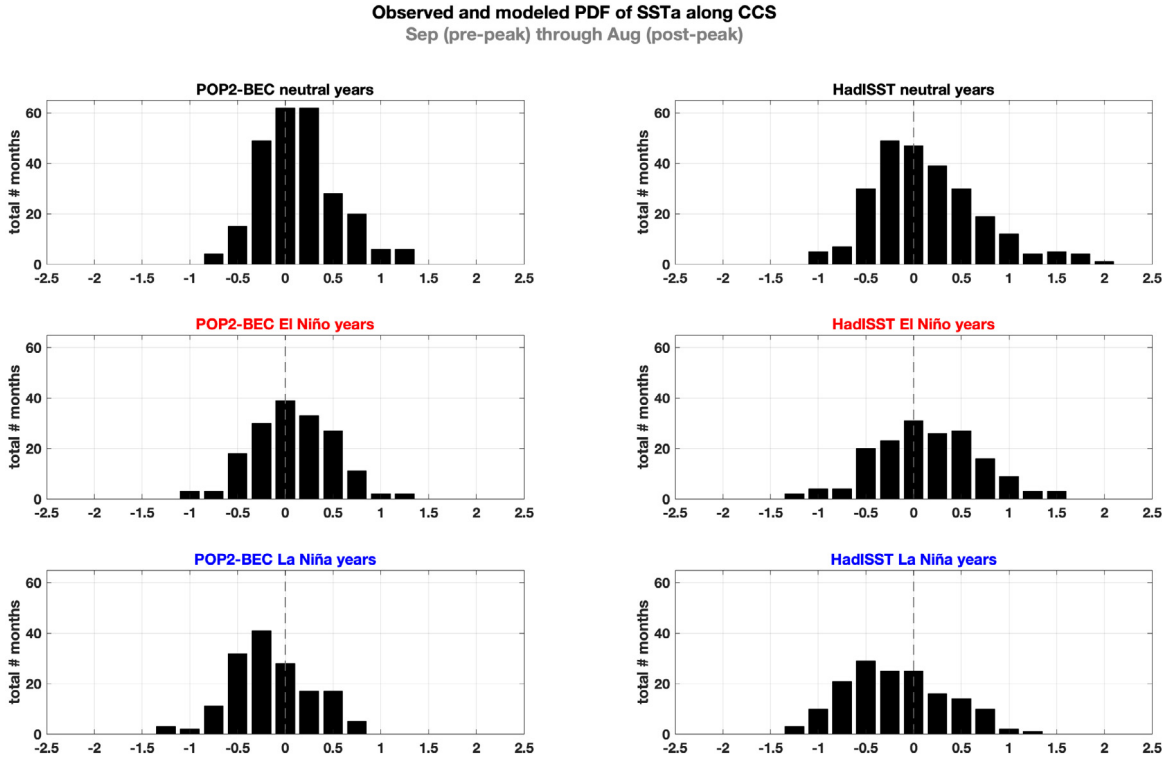

Fig. 20. Histograms of modeled (left) and observed (right) SSTa for pre-peak September through post-peak August over CCS for neutral, El Niño, and La Niña years. Model neutral years have a mean (μ) of 0.13 and a STD (σ) of 0.40, while observed neutral years have $\mu = 0.14$ and $\sigma = 0.57$. Model warm events ($\mu = 0.08$, $\sigma = 0.41$), have 57% of their months positive, while model cold events ($\mu = -0.15$, $\sigma = 0.41$) have 68% of their months negative. Observed warm events ($\mu = 0.15$, $\sigma = 0.55$) have 60% of their months positive, while observed cold events ($\mu = -0.18$, $\sigma = 0.53$) have 65% of their months negative.

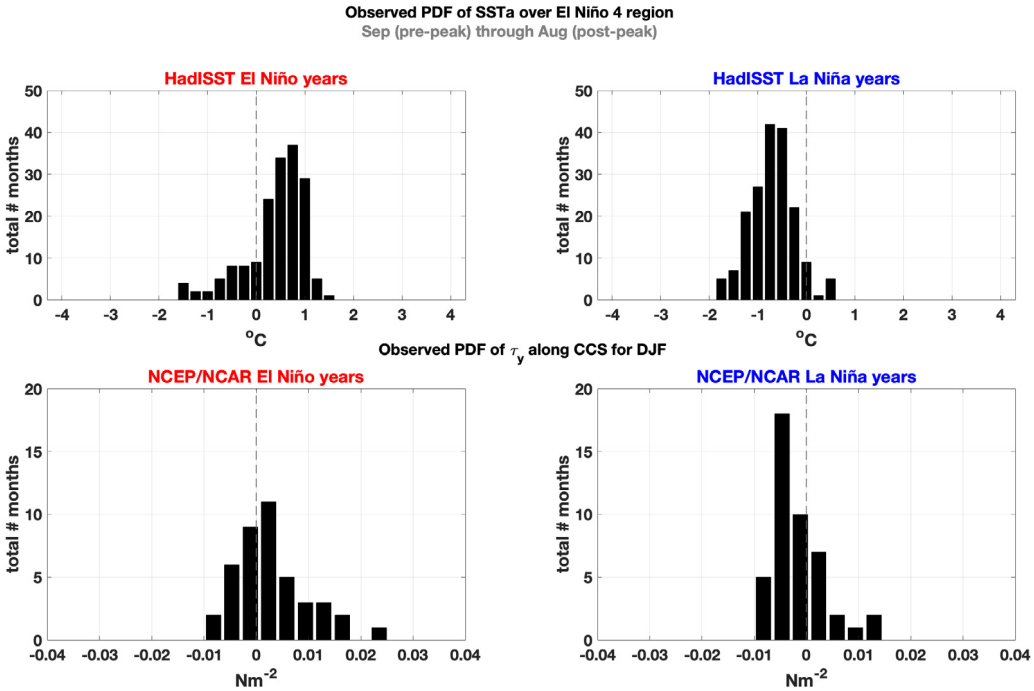

Fig. 21. Histograms of observed SSTa during December–January–February over Niño-4 Region in the Tropical Pacific (top panels). Histogram of meridional wind stress over CCS for the same period (bottom panels). Observed warm events ($\mu = 0.4$, $\sigma = 0.61$) have 79% of their months positive, while observed cold ($\mu = -0.7$, $\sigma = 0.46$) events have 94% of their months negative. Observed meridional CCS wind stress during warm events ($\mu = 0.0027$, $\sigma = 0.0071$) have 64% of their months downwelling favorable, while cold events ($\mu = -0.0017$, $\sigma = 0.005$) have 71% of their months upwelling favorable.

the scientists who attended the U.S. CLIVAR "Workshop on Forecasting ENSO Impacts on Marine Ecosystems of the US West Coast" held at SIO in 2016. We thank Matthew Long for granting access to the POP2-BEC simulation used in this study, and for providing important feedback on the manuscript. We thank the four anonymous referees who provided extensive and insightful comments that significantly improved the clarity and interpretation of our results in this manuscript.

References

Alexander, M.A., Bladé, I., Newman, M., Lanzante, J.R., Lau, N.C., Scott, J.D., 2002. The atmospheric bridge: The influence of ENSO teleconnections on air-sea interaction over the global oceans. J. Clim. 15, 2205–2231.

An, S.I., Jin, F.F., 2004. Nonlinearity and asymmetry of ENSO. J. Clim. 17, 2399–2412.

Ashok, K., Behera, S.K., Rao, S.A., Weng, H., Yamagata, T., 2007. El Niño Modoki and its possible teleconnections. J. Geophys. Res. 112, C11007.

Bakun, A., Black, B.A., Bograd, S.J., Garcia-Reyes, M., Miller, A.J., Rykaczewski, R.R., Sydeman, W.J., 2015. Anticipated effects of climate change on coastal upwelling ecosystems. Curr. Clim. Change Rep. 1, 85–93.

Barsugli, J.J., Sardeshmukh, P.D., 2002. Global atmospheric sensitivity to tropical SST anomalies throughout the Indo-Pacific Basin. J. Clim. 15, 3427–3442.

Bograd, S.J., Lynn, R.J., 2001. Physical-biological coupling in the California Current during the 1997-1998 El Niño-La Niña cycle. Geophys. Res. Lett. 28, 275–278.

Bograd, S.J., Lynn, R.J., 2002. Long-term variability in the Southern California Current System. Deep-Sea Res. II 50, 2355–2370.

Burgers, G., Stephenson, D.B., 1999. The normality of El Niño. Geophys. Res. Lett. 26, 1027–1030.

Cai, W., Wang, G., DeWitte, B., Wu, L., Santoso, A., Takahashi, K., Yang, Y., Carréric, A., McPhaden, M.J., 2018. Increased variability of eastern Pacific El Niño under greenhouse warming. Nature 564, 201–206.

Capotondi, A., Sardeshmukh, P.D., Di Lorenzo, E., Subramanian, A., Miller, A.J., 2019. Predictability of US West Coast Ocean Temperatures is not solely due to ENSO. Sci. Rep. 9, 10993. http://dx.doi.org/10.1038/s41598-019-47400-4.

Capotondi, A., Wittenberg, A.T., Newman, M., Di Lorenzo, E., Yu, J.-Y., Braconnot, P., Cole, J., DeWitte, B., Giese, B., Guilyardi, E., Jin, F.-F., Karnauskas, K., Kirtman, B., Lee, T., Schneider, N., Xue, Y., Yeh, S.-W., 2015. Understanding ENSO diversity. Bull. Amer. Meteorol. Soc. 96, 921–938.

Chávez, F.P., Coauthors, 2002. Biological and chemical consequences of the 1997–1998 El Niño in central California waters. Prog. Oceanogr. 54, 205–232. http://dx.doi.org/10.1016/S0079-6611(02)00050-2.

Chávez, F.P., Messié, M., 2009. A comparison of Eastern Boundary Upwelling Ecosystems. Prog. Oceanogr. 83, 80–96. http://dx.doi.org/10.1016/j.pocean.2009.07.032.

Checkley, D.M., Barth, J.A., 2009. Patterns and processes in the California Current System. Prog. Oceanogr. 84, 49–64.

Chelton, D.B., DeSzoeke, R.A., Schlax, M.G., El Naggar, K., Siwertz, N., 1998. Geographical variability of the first baroclinic rossby radius of deformation. J. Phys. Oceanogr. 28 (3), 433–460.

Chenillat, F., Rivière, P., Capet, X., Di Lorenzo, E., Blanke, B., 2012. North Pacific Gyre Oscillatino modulates seasonal timing and ecosystem functioning in the California Current upwelling system. Geophys. Res. Lett. 39, L01606. http://dx.doi.org/10.1029/2011GL049966.

Collins, C.A., Pennington, J.T., Castro, C.G., Rago, T.A., Chávez, F.P., 2003. The California Current system off Monterey, California: physical and biological coupling. Deep-Sea Res. II 50, 2389–2404.

Crawford, W., 2017. Investigations of the California Current System: Climate Variability and Advances in Modeling the Circulation (Ph.D. Dissertation). UC, Santa Cruz, p. 224.

Crawford, W.J., Moore, A.M., Jacox, M.G., Fiechter, E., Edwards, C.A., 2017. A resonant response of the California Current circulation to forcing by low frequency climate variability. Deep-Sea Res. II 151, 16–36.

Curchitser, E.N., Batchelder, H.P., Haidvogel, D.B., Fiechter, J., Runge, J., 2013. Advances in physical, biological, and coupled ocean models during the US GLOBEC program. Oceanography 26, 54–69.

Danabasoglu, G., Bates, S.C., Briegleb, B.P., 2012. The CCSM4 ocean component. J. Clim. 25, 1361–1389. http://dx.doi.org/10.1175/JCLI-D-11-00091.1.

Deser, C., Simpson, I., Phillips, A., McKinnon, K.A., 2018. How well do we know ENSO's climate impacts over North America, and how do we evaluate models accordingly? J. Clim. 31, 4991–5014.

Di Lorenzo, E., Cobb, K.M., Furtado, J.C., Schneider, N., Anderson, B.T., Bracco, A., Alexander, M.A., Vimont, D.J., 2010. Central Pacific El Niño and decadal climate change in the North Pacific Ocean. Nat. Geosci. 3, 762–765.

Di Lorenzo, E., Combes, V., Keister, J.E., Strub, P.T., Thomas, A.C., Franks, P.J.S., Ohman, M.D., Furtado, J.C., Bracco, A., Bograd, S.J., Peterson, W.T., Schwing, F.B., Chiba, S., Taguchi, B., Hormazabal, S., Parada, C., 2013. Synthesis of pacific ocean climate and ecosystem dynamics. Oceanography 26, 68–81.

Di Lorenzo, E., Miller, A.J., 2017. A framework for ENSO predictability of marine ecosystem drivers along the US West Coast. US CLIVAR Variations 15, 1–7.

Di Lorenzo, E., Miller, A.J., Schneider, N., McWilliams, J.C., 2005. The warming of the California Current: Dynamics and ecosystem implications. J. Phys. Oceanogr. 35, 336–362.

Dommenget, D., Bayr, T., Frauen, C., 2013. Analysis of the non-linearity in the pattern and time evolution of El Niño Southern Oscillation. Clim. Dyn. 40, 2825–2847.

Fiedler, P.C., Mantua, N.J., 2017. How are warm and cool years in the California Current related to ENSO? J. Geophys. Res. Oceans 122 (7), 5936–5951. http://dx.doi.org/10.1002/2017JC013094.

Fisher, J.L., Peterson, W.T., Rykaczewski, R.R., 2015. The impact of El Niño events on the pelagic food chain in the northern California Current. Global Change Biol. 21, 4401–4414.

Franks, P.J.S., Di Lorenzo, E., Goebel, N.L., Chenillat, F., Riviere, P., Edwards, C.A., Miller, A.J., 2013. Modeling physical-biological responses to climate change in the California Current System. Oceanography 26, 26–33.

Frischknecht, M., Munnich, M., Gruber, N., 2015. Remote versus local influence of ENSO on the California Current System. J. Geophys. Res. Oceans 120, 1353–1374.

Frischknecht, M., Munnich, M., Gruber, N., 2017. Local atmospheric forcing driving an unexpected California Current System response during the 2015-2016 El Niño. Geophys. Res. Lett. 44, 304–311.

Frischknecht, M., Münnich, M., Gruber, N., 2018. Origin, supply, production and fate: The three-dimensional biological pump in the California Current System. J. Geophys. Res. Oceans 123, 7939–7962.

Geider, R.J., MacIntyre, H.L., Kana, T.M., 1997. Model of phytoplankton growth and acclimation: responses of the balanced growth rate and the chlorophyll a: carbon ratio to light, nutrient-limitation and temperature. Mar. Ecol. Prog. Ser. 148, 187–200.

Geider, R.J., MacIntyre, H.L., Kana, T.M., 1998. A dynamic regulatory model of phytoplankton acclimation to light, nutrients, and temperature. Limnol. Oceanogr. 43, 679–694.

Gershunov, A., Barnett, T.P., 1998. ENSO influence on intraseasonal extreme rainfall and temperature frequencies in the contiguous United States: Observations and model results. J. Clim. 11, 1575–1586.

Goebel, N.L., Edwards, C.A., Zehr, J.P., Follows, M.J., 2010. An emergent community ecosystem model applied to the California Current System. J. Mar. Syst. 83, 221–241.

Griffies, S., Biastoch, C., Bryan, F., Danabasoglu, G., Chassignet, E.P., England, M.H., Gerdes, R., Haak, H., Hallber, R.W., Hazeleger, W., Jungclaus, J., Large, W.G., Madec, F., Pirani, A., Samuels, B., Sheinert, M., Gupta, A.S., Severijns, C.A., Simmons, H.L., Treguier, A.M., Winton, M., Yeager, S., Yin, J., 2009. Coordinated ocean-ice reference experiments (CORE). Ocean Model. 26, 1–46.

Gruber, N., Lackhar, Z., Frenzel, H., Marchesiello, P., Münnich, M., McWilliams, J.C., Nagai, T., Plattner, G.-K., 2011. Eddy-induced reduction of biological production in eastern boundary upwelling systems. Nat. Geosci. 4, 787–792. http://dx.doi.org/10.1038/NGEO1273.

Hickey, B.M., 1998. Coastal oceanography of western North America from the tip of Baja California to Vancouver Island. In: Robinson, A.R., Brink, K.H. (Eds.), The Sea, the Global Coastal Ocean: Regional Studies and Syntheses. J. Wiley and Sons Inc, New York, pp. 345–391.

Hickey, B.M., Banas, N.S., 2008. Why is the northern end of the California Current System so productive? Oceanography 21, 90–107.

Hsieh, W., 1983. The free kelvin wave in finite-difference numerical models. J. Phys. Oceanogr. 13 (8), 1383–1397.

Hurrell, J.W., Holland, M.M., Gent, P.R., Ghan, S., Kay, J.E., Kushner, P.J., Marque, J.-F., Large, W.G., Lawrence, D., Lindsay, K., Lipscomb, M.C., Mahowald, N., Marsh, D.R., Neale, R.B., Rasch, P., Vavrus, S., Vertenstein, M., Bader, D., Collings, W.D., Hack, J.J., Kiehl, J., Marshall, S., 2012. The community earth system model: A framework for colaborative research. Bull. Am. Meteorol. Soc. 94, 1339–1360. http://dx.doi.org/10.1175/BAMS-D-12-00121.1.

Jacox, M.G., Alexander, M.A., Stock, C.A., Hervieux, G., 2017. On the skill of seasonal sea surface temperature forecasts in the California Current System and its connection to ENSO variability. Clim. Dynam. 1–15. http://dx.doi.org/10.1007/s00382-017-3608-y.

Jacox, M.G., Fiechter, J., Moore, A.M., Edwards, C.A., 2015. ENSO and the California Current coastal upwelling response. J. Geophys. Res. Oceans 120, 1691–1702.

Jacox, M.G., et al., 2016. Impacts of the 2015–2016 El Nino on the California Current system: early assessment and comparison to past events. Geophys. Res. Lett. 43, 7072–7080.

Jahn, A., Sterling, K., Holland, M.M., Kay, J.E., Maslanik, J.A., Bitz, C.M., Bailey, D.A., Stroeve, E.C., Lipscomb, W.H., Pollak, D.A., 2011. Late-twentieth-century simulationof arctic sea ice and ocean properties in the CCSM4. J. Clim. 25, 1431–1452. http://dx.doi.org/10.1175/JCLI-D-11-00201.1.

Kilpatrick, T., Xie, S.-P., Miller, A.J., Schneider, N., 2018. Satellite Observations of enhanced chlorophyll variability in the Southern California Bight. J. Geophys. Res. Oceans 123, 7550–7563.

Kim, H.-J., Miller, A.J., 2007. Did the thermocline deepen in the souther California Current after the 1976-1977 climate regime shift? J. Phys. Oceanogr. 37, 1733–1739.

Kim, H.-J., Miller, A.J., McGowan, J., Carter, M.L., 2009. Coastal phytoplankton blooms in the Southern California Bight. Prog. Oceanogr. 82, 137–147.

Large, W.G., Yeager, S., 2009. The global climatology of an interannually varying airsea flux data set. Clim. Dyn. 33, 341–364.

Levine, A.F.Z., Jin, F.F., McPhaden, M.J., 2016. Extreme noise-extreme El Niño: How state-dependent noise forcing creates El Niño-La Niña asymmetry. J. Clim. 29, 5483–5499.

Lilly, L., Ohman, M., 2018. CCE IV: El Niño-related zooplankton variability in the southern California Current System. Deep-Sea Res. 120, 36–51.

Lynn, R.J., Simpson, J.J., 1987. The California current system: The seasonal variability of tis physical characteristics. J. Geophys. Res. 92, 947–966.

McGowan, J.A., Bograd, S.J., Lynn, R.J., Miller, A.J., 2003. The biological response to the 1977 regime shift in the California Current. Deep-Sea Res. 50, 2567–2582.

McGowan, J.A., Cayan, D.R., Dorman, L.M., 1998. Climate-ocean variability and ecosystem response in the northeast Pacific. Science 281, 210–217.

McPhaden, M.J., Busalacchi, A.J., Cheney, R., Donguy, J.-R., Gafe, K.S., Hapern, D., Ji, M., Julian, P., Meyers, G., Mitchum, G.T., Niiler, P.P., Picaut, J., Reynolds, R.W., Smith, N., Takeuchi, K., 1998. The Tropical Ocean-Global Atmopshere observing system: A decade of progress. J. Geophys. Res. 103, 14, 169–14, 420.

Miller, A.J., Song, H., Subramanian, A.C., 2015. The physical oceanographic environment during the CCE-LTER Years: Changes in climate and concepts. Deep-Sea Res. 112, 6–17.

Moore, J.K., Doney, S., Kleypas, J., Glover, D., Fung, I., 2002. An intermediate complexity marine ecosystem model for the global domain. Deep-Sea Res. II 49, 403–462.

Moore, J.K.J., Doney, S.C., Lindsay, K., 2004. Upper ocean ecosystem dynamics and iron cycling in a global three-dimensional model. Glob. Biogeochem. Cycles 18, GB4028. http://dx.doi.org/10.1029/2004GB002220.

Moore, J.K., Lindsay, K., Doney, S.C., Long, M.C., Misumi, K., 2013. Marine ecosystem dynamics and biogeochemical cycnling in the commnunity earth system model [CESM1(BGC)]: Comparison of the 1990s with the 2090s under the RCP4.5 and RECP8.5 scenarios. J. Clim. 26, 9291–9312. http://dx.doi.org/10.1175/JCLI-D-12-00566.1.

Newman, M., Alexander, M.A., Ault, T.R., Cobb, K.M., Deser, C., Di Lorenzo, E., Mantua, N.J., Miller, A.J., Minobe, S., Nakamura, H., Schneider, N., Vimont, D.J., Phillips, A.S., Scott, J.D., Smith, C.A., 2016. The Pacific Decadal Oscillation, revisited. J. Clim. 29, 4399–4427.

Niebauer, H.J., 1988. Effects of El Niño-Southern Oscillation and North Pacific weather patterns on interannual variability in the subarctic Bering Sea. J. Geophys. Res. 93, 5051–5068.

Ohman, M.D., 2018. Introduction to collection of papers on the response of the southern California Current Ecosystem to the Warm Anomaly and El Niño, 2014–16. Deep-Sea Res. 140, 1–3.

Ohman, M.D., Barbeau, K., Franks, P.J.S., Goericke, R., Landry, M.D., Miller, A.J., 2013. Ecological transitions in a coastal upwelling ecosystem. Oceanography 26, 210–219.

O'Reilly, J.L., Maritorena, S., O'Brien, M.C., Siegel, D.A., Toole, D., David Menzies, D., Smit, R.C., Mueller, J.E., Mitchell, B.G., Kahru, M., Chavez, S.P., Strutton, P., Cota, G.F., Hooker, S.B., McClain, C.R., Carder, K.L., Müller-Karger, F., Harding, R., Magnuson, A., Phinney, D., Moore, G.F., Aiken, J., Arrigo, K.R., Letelier, R., Culver, M., 2000. SeaWiFS Postlaunch Calibration and Validation Analyses, Part 3. NASA Tech. Memo. 2000-206892, 11, S.B. Hooker and E.R. Firestone, Eds. NASA Goddard Space Flight Center.

Rayner, N.A., Parker, D.E., Horton, E.B., Folland, C.K., Alexander, L.V., Rowell, D.P., 2003. Global analyses of sea surface temperature, sea ice, and night marine air temperature since the late nineteenth century. J. Geophys. Res. 108, 4407. http://dx.doi.org/10.1029/2002JD002670.

Rodgers, K.B., Friederichs, P., Latif, M., 2004. Tropical pacific decadal variability and its relation to decadal modulations of ENSO. J. Climate 17, 3761–3774. http://dx.doi.org/10.1175/1520-0442(2004)017<3761:TPDVAI>2.0.CO;2.

Rudnick, D.L., Zaba, K.D., Todd, R.E., Davis, R.E., 2017. A climatology of the California Current System from a network of underwater gliders. Prog. Oceanogr. 154, 64–106.

Schwing, F.B., Palacios, D.M., Bograd, S.J., 2005. El Niño impacts on the California Current ecosystems. U.S. CLIVAR Newsl. 3 (2), 5–8.

Small, J., Curchitser, E., Hedstrom, K., Kauffman, B., Large, W., 2015. The benguela upwelling system: Quantifying the sensitivity to resolution and coastal wind representation in a global climate model. J. Clim. 28, 9409–9432.

Song, H., Miller, A.J., Cornuelle, B.D., Di Lorenzo, E., 2011. Changes in upwelling and its water sources in the California Current System driven by different wind forcing. Dyn. Atmos. Oceans 52, 170–191.

Thomas, A.C., Brickley, P., Weatherbee, R., 2009. Interannual variability in chlorophyll concentrations in the Humboldt and California Current Systems. Prog. Oceanogr. 83, 386–392.

Thomas, A.C., Strub, P.T., Weatherbee, R.A., James, C., 2012. Satellite views of Pacific chlorophyll variability: Comparisons to physical variability, local versus nonlocal influences and links to climate indices. Deep-Sea Res. II 77–80, 99–106.

Turi, G., Alexander, M., Lovenduski, N., Capotondi, A., Scott, J., Stock, C., Dunne, J., John, J., Jacox, M., 2018. Response of Oxygen and PH to ENSO of the California Current System in a high-resolution global climate model. Ocean Sci. 14, 69–86.

Van Oostende, N., Dussin, R., Stock, C.A., Barton, A.D., Curchitser, E., Dunne, J.P., Ward, B.B., 2018. Simulating the ocean's chlorophyll dynamic range from coastal upwelling to oligotrophy. Prog. Oceanogr. 168, 232–247. http://dx.doi.org/10.1016/j.pocean.2018.10.009.

Wang, H., Kumar, A., Wang, W., Jha, B., 2012. U.S. summer precipitation and temperature patterns following the peak phase of El Niño. J. Clim. 25, 7204–7215.

Yeager, S.G., Danabasoglu, G., Rosenbloom, N.A., Strand, W., Bates, S.C., Meehl, G.A., Karspeck, A.R., Lindsay, M.C., Teng, H., Lovenduski, N.S., 2018. Predicting near-term changes in the earth system, a large ensemble of initialized decadal prediction simulations using the Commnity Earth System Model. http://dx.doi.org/10.1175/BAMS-D-17-0098.1.